

# Synthesis and Applications of Graphene and Its Nanocomposites



Mohd Asif and Irfan Ahmad

**Abstract** Graphene has been a material of interest, especially since the discovery of its free-standing form in 2003. The discovery provided hope to researchers looking for breakthroughs in the field that had not seen significant growth for long. Incremental improvements are not enough to meet the exponentially growing demands for cheap, convenient, and high-performing technologies. Graphene has the potential to provide new ways of achieving goals that previously seemed impossible by redefining the frontiers of science. It is because of the unprecedented material properties of graphene that were never demonstrated before by any other material. Novel and better material properties open up doors to new technologies and advancements in existing ones. However, it is imperative to obtain the material of suitable quality at a reasonable cost for it to compete with prevailing alternatives. In this chapter, various methods for synthesizing graphene have been discussed with a particular focus on the liquid-phase exfoliation (LPE) of graphite. Characterization with Raman spectroscopy, electron diffraction, and microscopy-based tools have been explored. The chapter also reviews applications of graphene in a few emerging areas. Graphene-based composites, with emphasis on their syntheses and applications, will be discussed.

**Keywords** Graphene synthesis · Liquid-phase exfoliation · Graphene characterization · Graphene applications

---

M. Asif

Interdisciplinary Nanotechnology Centre (INC), ZHCET, Aligarh Muslim University (AMU), Aligarh UP-202002, India

Department of Electrical Engineering, Indian Institute of Technology Delhi (IITD), New Delhi-110016, India

I. Ahmad (✉)

School of Engineering Science and Technology (SEST), Jamia Hamdard, New Delhi-110062, India

e-mail: [i.ahmad@alientt.com](mailto:i.ahmad@alientt.com)

## 1 Introduction

Carbon is one of the critical elements for sustaining life on earth and has so many compounds that a complete branch of chemistry has been dedicated to it. Pure carbon itself has several naturally occurring allotropes, and numerous others can be synthetically made in a laboratory. One such naturally occurring allotrope is graphite, in which atomically thin layers are stacked together by van der Waals forces. These individual layers are called graphene, where the ending term 'ene' marks the existence of  $sp^2$  bonding within the sheet plane. Atoms in graphene are bound together in a honeycomb-like structure, with six carbon atoms forming a hexagon. Three out of four valance electrons of each carbon atom make strong covalent  $\sigma$ -bonds with other carbon atoms. The remaining one electron per atom contributes to  $\pi$ -bonding, responsible for graphene's aromaticity and unique electronic properties [1]. It has been found that two  $\pi$ -electrons per ring are delocalized in graphene, making it different from other aromatic compounds such as benzene [2]. Graphene has been theoretically explored by many researchers for more than the past seven decades. The first theoretical explanation of graphene is dated back to 1947, when Canadian theoretical physicist P.R. Wallace studied the band structure of graphite [3]. Though Wallace did not use the term 'graphene', his contribution is regarded as the basis of theoretical studies of graphene.

For numerous decades, researchers tried to obtain free-standing single-layer graphene, while another section of theirs believed that it was practically impossible. The discrepancy came to an end in 2004, when K.S. Novoselov et al. reported successful isolation of single-layer graphene (SLG) from graphite [4]. The discovery of free-standing graphene and subsequent experiments by K.S. Novoselov and A. Geim won them a Nobel in physics in 2010. Controversy followed the award and W.A. de Heer of Georgia Tech., who had also contributed significantly to graphene science, wrote a letter to the Nobel committee stating that "The Nobel Prize committee did not do its homework" [5]. Nevertheless, graphene had been studied extensively and had demonstrated tremendous potential in multiple applications by that time because of its exceptional properties.

The exotic properties arise broadly due to single-layer thickness and  $sp^2$  hybridization of electronic orbitals in graphene. The most interesting ones are high electrical conductivity ( $>10^6$  S/m) [6] very high thermal conductivity (up to  $\sim 5300$  Wm $^{-1}$  K $^{-1}$ ), [7] highest ever measured mechanical strength ( $\sim 130$  GPa) and Young's modulus ( $\sim 1$  TPa), [8] extremely high experimentally calculated carrier mobility ( $\sim 2 \times 10^5$  cm $^2$ V $^{-1}$  s $^{-1}$  for suspended graphene), [9] and very high theoretical specific surface area of ( $\sim 2630$  m $^2$ g $^{-1}$ ) [10].

The high carrier mobility is due to the conical band structure of SLG, in which the highest occupied molecular orbital (HOMO) and lowest unoccupied molecular orbital (LUMO) meet each other at Dirac points (vertices of the Dirac cones) [3]. It is a well-known fact that the effective mass of charge carriers is inversely proportional to the curvature of the band, and at the Dirac points, the curvature is very high (ideally infinite), making electrons massless fermions (ideally). Carrier mobility is inversely

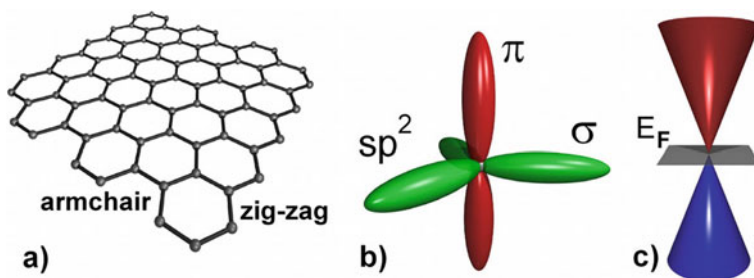


**Fig. 1** Representative images of (a) hexagonal structure of graphene and chirality, (b)  $sp^2$  hybridization with sigma and pi bonding electrons, and (c) valence and conduction bands meeting each other at a Dirac point [11]

related to its effective mass hence such high mobility is observed in graphene. Due to the unique band-structure of graphene, it has been called by multiple names, such as zero-bandgap semiconductor and zero-overlap semimetal. The high electrical conductivity of graphene is due to delocalized  $\pi$ -electrons that are free to roam throughout the sheet [11]. The magnificent mechanical properties arise due to  $sp^2$  hybridization of orbitals, resulting in stronger bonding between hexagonally organized carbon atoms [12]. Representative images of hexagonal structure,  $\sigma$  and  $\pi$  bonds, and Dirac cones for graphene are shown in Fig. 1.

The thermal conductivity of materials increases with bond strength between their constituent atoms [13]. The outstanding thermal conductivity of graphene is, thus, attributed to very strong  $sp^2$  bonding between carbon atoms [14]. High thermal conductivity and very high mechanical strength is an excellent combination for heat sinks in electronic circuits and devices [15]. Another compelling property of an SLG is its light absorption, measured to be 2.3% [16]. A single layer with such a high conductivity and good transparency makes it a suitable candidate for transparent electrodes for optoelectronic devices [17].

The properties of materials degrade with their quality, and for a material with such unique properties, high-quality synthesis is challenging. Often, researchers seek an optimization between quality and cost (quantity). Various methods have been developed to obtain graphene, and graphene's quality varies with its synthesis route. Some commonly used methods are epitaxial growth, [18] chemical vapor deposition (CVD), [19] and exfoliation of graphite [20]. Graphite exfoliation-based techniques are more promising for producing large quantities with reasonable quality. The quality assessment is the next step after the synthesis, for which various tools and methods are employed. Raman spectroscopy is one of the most reliable techniques for acquiring scores of information on synthesized graphene. It provides information regarding the number of layers, [21] defects, [22, 23] doping, [23] chirality, [24] etc., as well as effects of external parameters such as pressure, [25] and temperature [26]. Other tools, for instance, selected area electron diffraction (SAED), and high-resolution transmission electron microscopy (HRTEM), are competent for analyzing crystallinity, defects, and the number of layers [27]. Atomic force microscopy (AFM)

is often used for the determination of electrical [28] and mechanical [29] properties in addition to quality evaluation.

In the recent past, graphene has become a material of interest in a vast spectrum of applications for commercialization. It has been, therefore, forecasted in a research report by an apex market experts group named IDTechEx that the graphene market will grow from < 100 M USD in 2020 to ~ 700 M USD in 2031 [30]. Graphene has been commercialized with several products currently available in the market such as automobile coating products by ‘Turtle Wax’, [31] sporting products by a leading sports goods manufacturer ‘Head’, [32] shoes by ‘inov-8’, [33] many products, especially face masks, by ‘G1 Wonders’, [34] tailor-made solutions for a range of industrial requirements by ‘Graphene XT’ [35]. There are numerous sectors where graphene is being explored, and the resulting products are expected to hit the market in the coming years.

Even though graphene itself is a wonder material with a wide range of applications, still in a large number of applications, graphene-based nanocomposites (NCs) are a better choice. Graphene has been investigated as the continuous phase (matrix) as well as dispersed phase (filler) when hybridized with diverse classes of materials, including metals, their oxides, and sulfides, and organic polymers. In-situ polymerization is the most common route for making polymer-graphene NCs. For metal-graphene NCs coatings, electrodeposition is commonly employed, while for their powdered forms, simultaneous reduction of metal ions and graphene oxide (GO) has been frequently reported. Graphene NCs with metal oxides and sulfides are usually produced by solvo-/hydro-thermal methods.

This chapter is dedicated to discussing various synthesis protocols, characterization techniques, and applications of graphene. Synthesis using CVD, epitaxial growth, and exfoliation of graphite will be briefly introduced. It will be followed by a detailed discussion on the LPE of graphite. Evaluation of the quality of graphene through characterization techniques, especially with Raman spectroscopy, will be elaborated. For the sake of completeness, crucial methods such as SAED and microscopic techniques will also be discussed. Potential applications of graphene in electronics, energy conversion and storage, environmental remediation, and healthcare sectors will be reviewed. NCs of graphene with polymers, metals, metal oxides, and metal sulfides will also be within the scope of this chapter. Finally, the chapter will be summarized, and future scopes will be highlighted to conclude the chapter.

## 2 Synthesis of Graphene

Properties of the synthesized graphene are dependent upon the preparation route it has undergone. Therefore, it is imperative to discuss major synthesis methods in order to understand the variation that may arise due to the preparation method. Commonly utilized synthesis routes are discussed in this section.

## 2.1 Epitaxial Growth

Epitaxial growth involves the deposition of a material layer onto a well-oriented substrate. Thermal decomposition of silicon carbide and molecular beam epitaxy (MBE) are the two most commonly employed methods for the epitaxial growth of graphene. The decomposition of SiC, when heated to high temperatures, and its structural studies were reported by D. Badami in 1962 [36]. In this approach, a crystal of hexagonal SiC is annealed at high temperatures of around 1000°C in an ultra-high vacuum (UHV) [37]. The high temperatures allow silicon atoms to sublime into the vacuum while carbon atoms, having lower vapor pressure than Si, [38] remain on the surface. The carbon atoms at the surface then rearrange into a hexagonal structure which is nothing but a graphene sheet. Two layers of SiC decompose to form a single layer of graphene [39]. Both SLG and few-layer graphene (FLG) can be grown with this method. Walt de Heer and his team studied the 2D electron gas of epitaxially grown graphene on the (0001) face of a 6H-SiC crystal [40]. This method is advantageous for the semiconductor industry because graphene inherently grows on an insulating SiC substrate. Disadvantages of the process include the limitation of synthesized graphene area by the SiC crystal size and the control over the number of graphene layers synthesized. Decomposition of SiC and subsequent graphene formation is represented schematically in Fig. 2.

Another frequently reported technique for growing graphene epitaxially is MBE. In this technique, carbon deposition occurs atom by atom on a substrate from the source material in the growth chamber under UHV (as shown in Fig. 3). The source of carbon atoms could be solid such as highly ordered pyrolytic graphite (HOPG), [41] or could even be a gas, such as acetylene ( $C_2H_2$ ) [42]. One significant advantage of this method is that graphene can be grown onto a variety of substrates. Researchers have demonstrated the use of metals, [43] insulators, [44] elemental semiconductors, [45] and metal oxides [46] as substrates. Films of another material (especially metals) can also be deposited onto the substrate before exposure to the beam of carbon atoms and the subsequent growth of graphene. The choice of substrate affects the quality of the graphene, and thus high-quality graphene can be grown with this approach [47]. Furthermore, MBE offers possibilities for in-situ growth monitoring and characterization of graphene sheets [48]. The growth process, however, is slow and takes tens of minutes to hours depending on the product requirements and thus

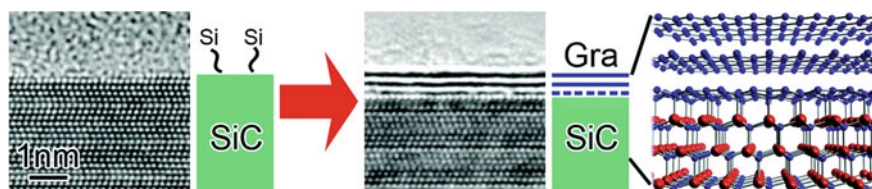


**Fig. 2** Formation of graphene via decomposition of SiC at {0001} surface; HRTEM images and schematic representation [37]

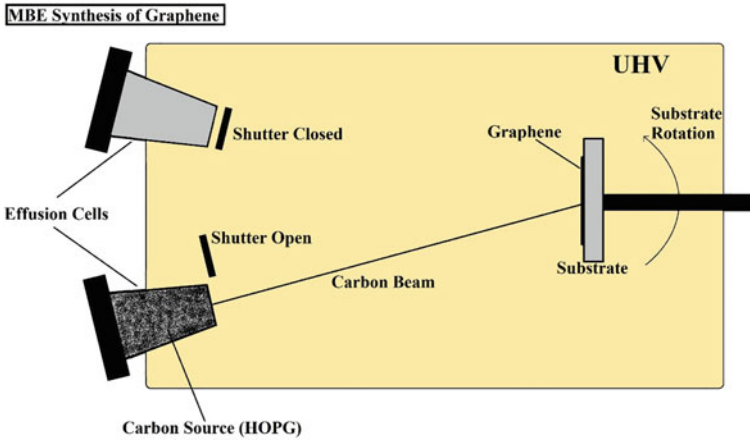


**Fig. 3** A schematic representation of the setup for MBE synthesis of graphene

low throughput, which is a major disadvantage of this method. Also, the process is costly, and therefore, it is generally reserved for applications where high-quality (pristine) graphene is the prime requirement.

## 2.2 Chemical Vapour Deposition (CVD)

CVD technique is the most commonly used technique for growing high-quality and large-area graphene sheets [49]. The process typically involves the adsorption of a carbon-containing (hydrocarbon) gas on a transition metal surface, its decomposition and removal of unwanted groups, and finally, the rearrangement of carbon atoms to form the honeycomb structure (Fig. 4 shows the schematics). Commonly used hydrocarbon gas precursors are ethylene, [50] methane, [51] and acetylene [52]. Several transition metals have been reported to perform as catalytic substrates such as Pt, [50, 53] Ni, [51, 54] Fe, [52] Cu [54]. The solubility of carbon in these metals at high temperatures affects the process. Dissolved carbon tends to segregate on the surface when cooled, and thus, an additional number of graphene layers are formed. Therefore, it becomes challenging to control the number of layers with the CVD process. Copper is considered the best amongst the metal substrates demonstrated so far for SLG due to the very poor solubility of carbon in it ( $<1$  C atom per  $10^5$  Cu atoms at  $1000$  °C), [55] which allows only chemical decomposition of hydrocarbon gas to form graphene. The first ‘single layer graphite’ (as they called it) through CVD was reported by T.A. Land et al. in 1992 on Pt(111) surface [53]. The process evolved considerably after Novoselov’s 2004 paper, and CVD has become one of the most promising techniques for obtaining large-area graphene. The crystallinity of a substrate is another critical parameter. Smooth and well-oriented single

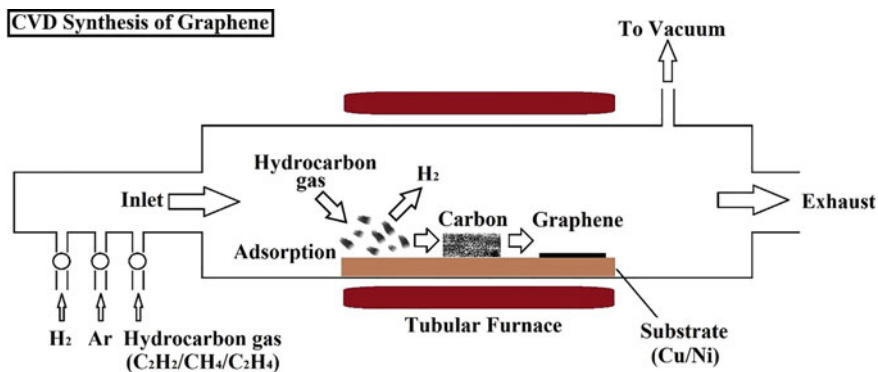


Fig. 4 Schematic representation of a typical CVD setup and process

crystal substrates are preferred for monolayer graphene because grain boundaries and other defects act as nucleation sites and thus stimulate the formation of multi-layer graphene (MLG) [56]. Hydrogen is generally used in the annealing step to remove the oxide layer, if any, from the catalyst surface. It is crucial to note that increasing the hydrogen:methane ratio in the feedstock reduces the graphene growth rate on Cu substrate while boosting the growth rate when Ni substrate is used [54]. It can be ascribed to the high hydrogen solubility and low carbon solubility in Cu, while the opposite is true for Ni. The quality of the produced graphene depends on the flow rate of the precursor gas, the transition metal used as the catalytic substrate, and chamber temperature. Growth can take place at relatively higher pressures with argon introduced into the system.

Two configurations, namely Thermal CVD (TCVD) and Plasma Enhanced CVD (PECVD) are commonly employed for graphene synthesis. TCVD process uses high temperatures of around 1000°C (close to the melting point of substrate metals) for the decomposition of hydrocarbon gas [51]. High temperatures, generally, favor the formation of highly crystalline wrinkle-free graphene sheets [50]. Hot wall CVD and cold wall CVD are two subclasses of TCVD. The entire growth chamber is heated in a hot-wall setup while only the substrate is heated in a cold-wall configuration. High throughput is an inherent advantage of cold wall CVD because the reactants are not deposited on the reactor walls, and thus it is more suitable for scale-up production. PECVD, on the other hand, is a deposition technique of substantially lower temperatures. The PECVD process for graphene synthesis has been reported at temperatures as low as 240°C [57]. The elimination of heating and cooling of the substrate in the PECVD process significantly reduces the synthesis time but at the cost of quality degradation of product material. In a typical setup, plasma is created, which reacts with the hydrocarbon gas to form more reactive radicalized species capable of forming a honeycomb lattice at relatively low temperatures. Li et al. studied the growth of graphene through the PECVD process on Cu substrate at different temperatures [58].

The CVD process is a reliable technique for synthesizing high-quality large-area graphene sheets. However, the transfer of the prepared graphene from metal substrates to other substrates is necessary for most applications. The transfer process is critical and leads to the degradation of the quality of graphene by introducing imperfections such as kinks, wrinkles, cracks, etc. [59]. Some techniques have also been developed for synthesizing graphene on non-metallic substrates such as glass, which can avoid transfer steps for multiple applications [60].

### 2.3 Exfoliation of Graphite

Graphite is a meticulous stack of graphene layers, and thus, free-standing graphene can be obtained by unstacking these layers. Exfoliation of graphite is just another term for unstacking it to obtain the graphene sheets. The energy required for exfoliation (or separation) of two  $1\text{nm}^2$  graphene sheets has been calculated to be around  $2\text{eV}$  [61]. Several methods have been explored by researchers for providing this energy to exfoliate graphite. Mechanical, liquid-phase, and electrochemical exfoliation methods have been reported more frequently in the literature.

Mechanical exfoliation was the first method used by Novoselov and Geim to obtain free-standing graphene [4]. They used scotch tape and a crystal of graphite for the purpose, and thus the technique is referred to as the “scotch-tape-method” in layman’s terms. In this experiment, a piece of tape is first pressed against a well-oriented HOPG crystal face and removed carefully. Due to this peeling process, many layers detach from the crystal and come off sticking onto the scotch tape. Another piece of scotch tape is then pressed against the first piece and then carefully separated, which results in the distribution of the detached layers onto these two pieces. The process is repeated multiple times until the desired number of layers remains on the tape. The pieces of scotch tape are then either put in a solution to remove epoxy and obtain free-standing graphene or on a silica slide to get graphene transferred onto a substrate.

The electrochemical exfoliation process generally involves a setup of two electrodes, one of which is graphite which could either be an anode or a cathode in a liquid electrolyte solution. When a voltage is applied across the two electrodes, ionic species intercalate between the layers of graphite, causing weakening of van der Waals attraction and thus dissociation of mono- and few-layer graphene from the graphite electrode into the solution [62]. Various geometries of graphite such as foils, flakes, rods, and discs have been studied for this purpose. Electrodes made up of HOPG were observed to be providing better quality graphene than naturally occurring forms [63]. DC voltages between 1 to 30V and low-frequency AC voltages up to 20V have been explored and reported [64]. Sulfuric acid is a commonly used electrolyte, which dissociates into  $\text{H}^+$  and  $\text{SO}_4^{2-}$  ions in an aqueous solution. Sulfate ions, compared to other anions, easily intercalate between the graphite layers causing them to exfoliate into graphene layers more efficiently [65]. High yield of around 50% was reported by J. Liu et al. by using vertical cell configuration [66]. Even



better results (65%) were obtained by T.C. Achee et al. with the help of a permeable and expandable container to make a compressed graphite electrode from graphite powder [67].

Another fundamental method is the oxidation of graphite flakes to obtain exfoliated and oxidized graphene called graphene oxide (GO), which is useful for numerous applications. It can also be used as a precursor for obtaining graphene through suitable reduction processes. Hummer's method is the most popular protocol for oxidation and exfoliation of graphite to convert it into GO [68]. The process is an age-old technique used for graphite oxide synthesis, but it kept on modifying over time. In a typical procedure, sulfuric acid is used for intercalation and potassium permanganate as the oxidizing agent, while hydrogen peroxide is used at a later stage of the process to eliminate excess permanganate. The material is then washed and dried to obtain yellowish water-soluble GO. Several methods have been developed to convert GO into graphene; chemical [69] and thermal [70] reduction are the most common amongst them. The obtained graphene is not pure or pristine as some functional groups remain attached to it. Thus, it is referred to as reduced graphene oxide (rGO).

Liquid phase methods use solvents such as water (with and without surfactants) and organic solvents to exfoliate graphene sheets from graphite flakes. Ultrasonication in a suitable solvent is the primary method used in this category. Other improvised methods wield a combination of mechanical techniques such as high energy ball milling (HEBM), shear mixing, and centrifugation, in addition to ultrasonication. Biological substances instead of synthetic surfactants have also been reported for LPE synthesis of graphene [71]. LPE methods will be discussed in more detail in the next section. Exfoliation synthesis, especially LPE, is one of the best techniques to obtain large quantities of quality graphene at an economical cost.

### 3 Liquid-Phase Exfoliation (LPE) Synthesis

Liquid phase exfoliation method has tremendous potential for scale-up production of graphene. It is a simple technique where mechanical energy is applied to exfoliate graphite flakes in a liquid medium. The energy could be provided through acoustic waves, shear force, or centrifugal force. Acoustic waves such as ultrasonic waves are applied through a liquid to transfer energy to graphite flakes which can stimulate the separation process and lead to the formation of graphene sheets. Surfactants are generally used to assist the exfoliation process by creating an electrostatic repulsive force between layers. Surfactant-free approaches, in which organic solvents are used instead of water for dispersing the graphite powder, also recurrently appear in the literature. Graphene is not dispersible in water but exhibits a high dispersion in many organic solvents, which provides a better possibility of its stability after exfoliation and hence a better yield. Organic solvents such as ortho-dichlorobenzene (ODCB) [72] and N-methyl-pyrrolidone (NMP) [73] have been reported quite often for synthesizing graphene through the LPE method. Further improvements were reported by the addition and tuning of the concentration of n-octylbenzene in the

former two organic solvents [74]. The primary stabilization mechanism, with or without surfactants, mainly involves a charge transfer between unstacked graphene and the stabilizing agents. The charge transfer, most of the time, takes place from electron-rich graphene to the stabilizer molecules, but the reverse can also happen (such as in the case of pyridine) [75].

M. Telkhozhayeva et al. studied in detail the ultrasonication-assisted exfoliation of graphite [76]. They explored the effect of the frequency of sonic vibrations on the quality of synthesized graphene and the efficiency of synthesis. They reported that good quality graphene (~30% monolayer and ~45% bi- and tri-layer) with an average lateral size of 13 $\mu$ m could be obtained in ethanolic bath sonication by increasing the frequency from the usually used 40kHz to a higher value of 80kHz. They demonstrated that increasing the frequency positively affects the exfoliation process and reduces the chances of inducing lattice defects in the synthesized graphene. The group also reported that bath sonication is a more efficient technique than probe sonication.

M. Monajjemi theoretically explored the LPE of graphite by ultrasonication [77]. Various types of surfactants and their effects on the efficiency of exfoliation were studied, and it was found that ionic surfactants are more efficient than others. The exfoliation efficiency in any dispersion medium can be written in descending order as cationic, anionic, zwitterionic, and non-ionic. It was further reported that the sulfonic group is very effective in assisting the exfoliation of graphite and stabilizing the produced graphene in solvents to prevent restacking.

Water-insoluble stabilizers have also shown potential for increasing the efficiency of LPE [78]. Y. Shin and group have recently demonstrated the use of pyrene derivatives such as bis-pyrene stabilizers functionalized with pyrrolidine, which can substantially improve the quality of obtained graphene. The use of toxic substances, however, limits its applications to the areas where biocompatibility is not a requirement.

A detailed experimental as well as theoretical study on LPE of graphite was performed by Coleman's group, which has greatly contributed to LPE research [79]. The study reveals three stages of the conversion of graphite into graphene through the sonication-assisted LPE process, namely: *Flake rupture and kink band formation; peeling off of thin graphite strips; and exfoliation to thin flakes*. In the first stage, acoustic waves travel through the graphite piece due to applied sonic energy, resulting in ridges forming on the graphite structure. These ridges have a large number of defects which increase the reactivity and thus the possibility of attachment of various functional groups. The ridges then crack in the second stage, and the exposed edges become oxygen-rich due to the addition of functional groups. The third and final stage mainly involves intercalation and peeling off the layers from the graphite structure and graphene dispersion into the solvent. The study has led to a very significant improvement in the basic understanding of the LPE process and is expected to improve the overall process as well. The three stages are schematically represented in Fig. 5.

A large number of organic and inorganic solvents have been reported for LPE of graphite since the discovery of free-standing graphene. A.B. Bourlinos et al., in 2009,

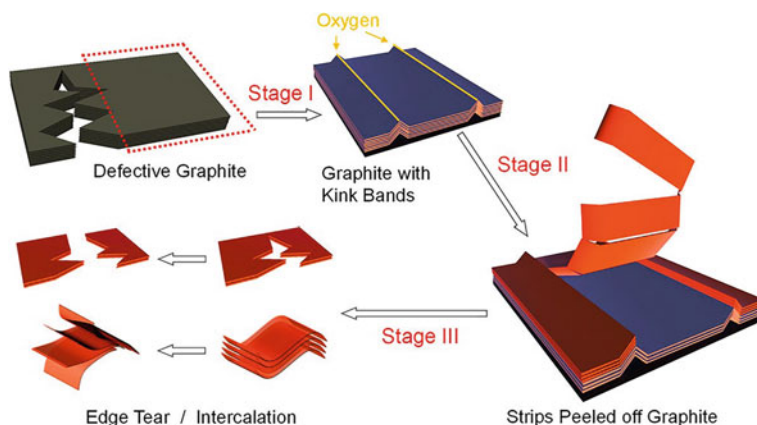


**Fig. 5** Three stages of LPE process [79]

added multiple new solvents to the list of already known solvents for LPE [75]. They experimented LPE with pyridine and some perfluorinated aromatic solvents such as hexafluoro-benzene ( $C_6F_6$ ), octafluoro-toluene ( $C_6F_5CF_3$ ), pentafluoro-benzonitrile ( $C_6F_5CN$ ), and pentafluoro-pyridine ( $C_5F_5N$ ).

A mixed solvent strategy was proposed by M. Yi et al. for exfoliating graphite powder to obtain graphene nanosheets [80]. They performed two experiments with mixtures of alcohol and water. Mixture-1 was prepared with ethanol in water, and mixture-2 with isopropyl alcohol in water. Mild sonication was employed to exfoliate nanosheets from graphite powder. The concentration of alcohols was varied to optimize the processes for maximum yield and better quality. The optimum concentration was reported to be 40% for mixture-1 and 55% for mixture-2, with a yield up to 10%. Simple strategies like this one could benefit upscale graphene production through LPE in the future.

D. Nuvoli and the team first used ionic liquids as solvents for graphite dispersion [81]. The team used grinding in mortar followed by ultrasonication and finally centrifugation for obtaining FLG. Ionic solvent 1-hexyl-3-methyl-imidazolium hexafluorophosphate was used with no other functionalizing compounds. They reported a very high dispersivity of graphene (5.33 mg/ml) in the solvent. One more advantage of this method is that the solvent can be processed for reuse, significantly reducing the production cost.

The addition of common organic salts during the LPE process has also been shown to have positive impacts. A group led by X. Jiang proposed using organic salts such as edetate disodium, sodium tartrate, potassium sodium tartrate, and sodium citrate in organic solvents to improve the exfoliation efficiency [82]. The group reported more than a hundred times improvement in efficiency with a mixture of dimethyl sulfoxide (DMSO) and sodium citrate.

A more sophisticated but effective 'lab on a chip' LPE was proposed by X. Qiu and associates [83]. They exploited a phenomenon called hydrodynamic cavitation,

which involves bubble generation and implosion in flowing liquid due to sudden changes in pressure, to induce the exfoliation of graphite. The setup, a microfluidic channel with a smaller orifice, was fabricated on a silicon wafer. A mixture of water, sodium cholate (surfactant), and graphite powder were forced to flow through the orifice, which resulted in a change in pressure of 10 bar. This local change in pressure stimulates the unstacking of graphene layers. A series of these microchannels can be fabricated on a silicon wafer for upscale production of graphene nanosheets.

HEBM processing of graphite powder is another crucial method within LPE genre for cost-effective high quality synthesis of graphene sheets. It has been reported by several researchers that the blending of inorganic materials such as NaCl [84] and sulfur [85] during the milling process improves the flake size and the quality of the synthesized graphene, owing to the intercalation of these particles acting as a wedge between the layers and thus assisting the exfoliation. However, M.F. Alam et al. reported that the blending of salt during the ball milling process results in the creation of defects in the synthesized graphene and the residual salt impurities degrade the overall quality of thus synthesized graphene [86]. The group used a combination of three techniques viz. ultrasonication, HEBM, and centrifugation, with and without inorganic salts (NaCl, KCl, and LiI). They compared the results obtained from these experiments and reported HEBM followed by three times centrifugation without salts to be the best combination for synthesizing high-quality sheets. The results are arranged in Table 1 as shown below:

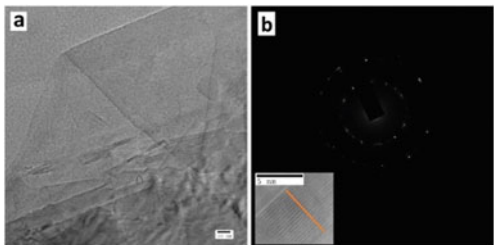
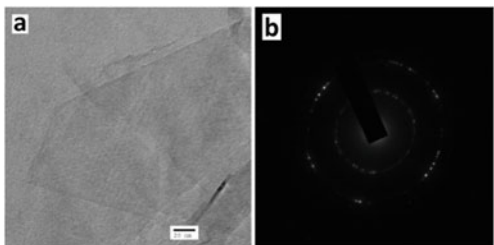
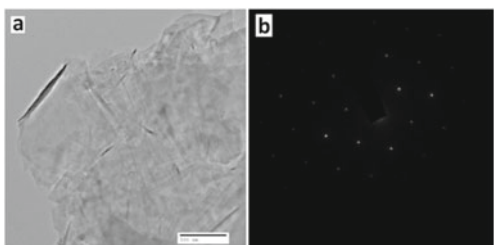
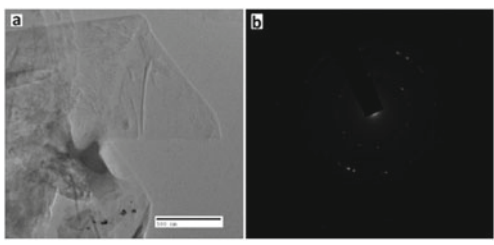
The above discussed results seem counter-intuitive as the earlier discussion in this section pointed out the intercalation of ions between the sheets acting as tiny wedges during LPE, thus making it easier to exfoliate the graphene sheets. The results in this part are with HEBM processing before the LPE step. With HEBM processing, blending of salt negatively impacts graphene synthesis.

## 4 Characterization of Graphene

### 4.1 Raman Spectroscopy

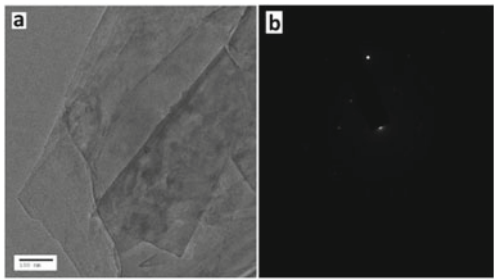
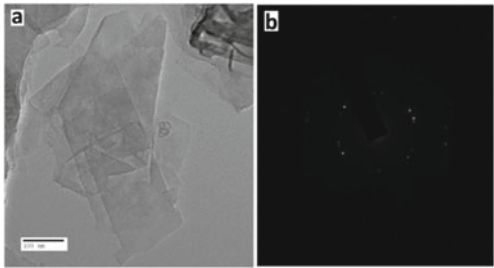
Raman (inelastic) scattering is so tiny compared to Rayleigh scattering (elastic) that its detection was practically impossible to be utilized in a probing technique until high-intensity lasers were invented. Raman spectroscopy has become a tool with extraordinary capabilities to probe molecules and crystals based on the Raman scattering phenomenon which takes place due to the vibrational and rotational modes of the material. The modes that change the polarizability of material are called Raman active modes, and the resulting output spectrum consists of bands of different intensities. A typical Raman instrument's output, a plot between intensity and Raman shift, gives information about the atoms and interatomic bondings that are signatures of a molecule, and thus, the technique acts as a molecular fingerprinting. This tool has

**Table 1** Summary of results by M.F. Alam et al. [86]

Preparation Method	Halide Used	Results (TEM and SAED)	Remarks
3 × Ultrasonication	None		Few 100 nm size, Fringes 0.33 nm, 2 prominent rings in SAED
HEBM + 3 × Ultrasonication	None		Few 100 nm size, 2 prominent 1 feeble rings in SAED, Lattice defects
HEBM + 3 × Centrifugation	None		Size in $\mu\text{m}$ , sixfold symmetry in SAED, Defect-free lattice
HEBM + 3 × Centrifugation	NaCl (40%)		Size in $\mu\text{m}$ , 2 prominent 1 feeble rings in SAED, multi-layer, Lattice defects

(continued)

**Table 1** (continued)

Preparation Method	Halide Used	Results (TEM and SAED)	Remarks
HEBM + 3 × Centrifugation	KCl (40%)		Multiple overlapping sheets, Asymmetric pattern in SAED, Inefficient method
HEBM + 3 × Centrifugation	LiI (40%)		Multiple overlapping sheets, 1 prominent 1 feeble ring in SAED, Lattice defects

been proven extremely useful for the characterization of honeycomb carbon materials. The technique is so sensitive that it can be used to analyze the electronic and phononic behavior in a single sheet of graphene, [87] a single CNT, [88] a single fullerene, [89] and any changes introduced in their structure. This section will mainly be focused on the Raman spectroscopy of graphene and the effects of the number of layers, defects, and doping on the spectrum.

Figure 6a shows a typical Raman spectrum of an SLG. Many bands arise due to Raman active phonons, but most result in a weak signal. It is, therefore, a common practice to study only four prominent bands, namely G, D, G', and D', for obtaining relevant information on the underlying material. These bands originate due to various phenomena occurring in graphene, which are illustrated in Fig. 6b. The information about these bands in the following paragraphs is for laser photon energy of 2.41eV (514nm wavelength).

The G band originates from in-plane C–C bond stretching vibrations and occurs at around  $1585\text{ cm}^{-1}$  due to first-order Raman scattering involving one phonon. The peak of the G band is an outcome of resonance and is a characteristic peak for honeycomb carbon materials. It is related to doubly degenerate phonon modes, namely, longitudinal optical (LO) and in-plane transverse optical (ITO) at the center of the first Brillouin zone. The G band is the only non-dispersive band (having no correlation between band position and photon energy) in the Raman spectrum

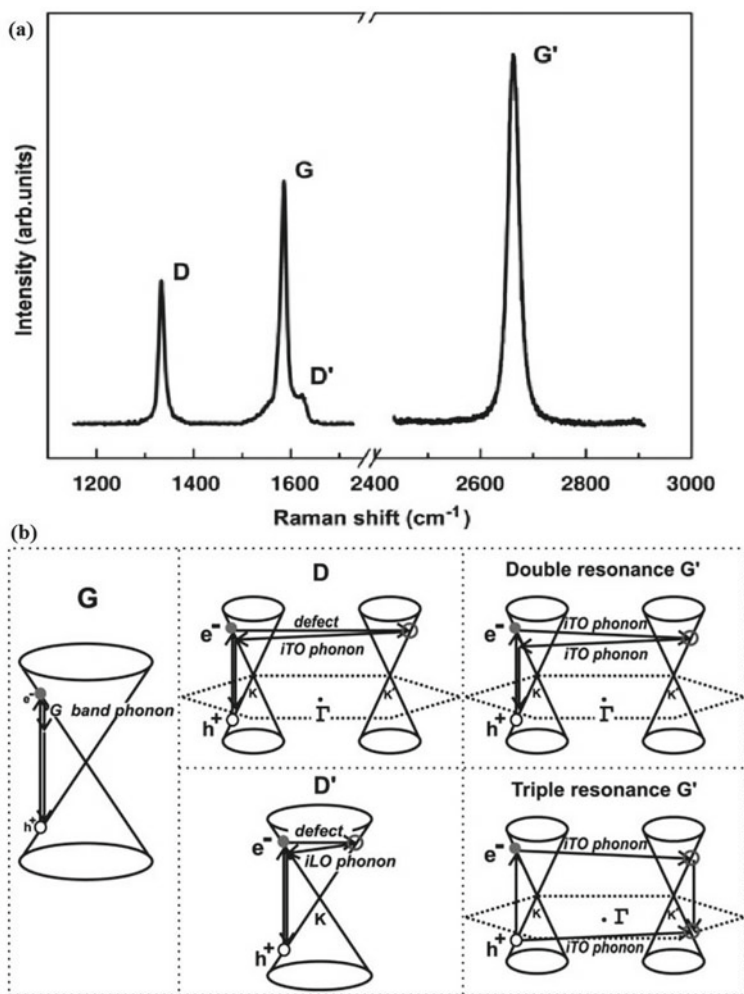


**Fig. 6** Raman spectrum of an SLG showing: various bands (a) and origin of these bands (b) [87]

of graphene. The G' band (also known as 2D band because it occurs at twice the Raman shift of D band) at around  $2700\text{ cm}^{-1}$  results from a second-order process involving two phonons participating in the Raman scattering of the excited electron. A double resonance process arising from inter/intra-valley scattering gives rise to this band in the spectrum. Triple resonance processes are also sometimes involved and are responsible for G' band. The G' band is a signature of  $sp^2$  hybridized carbon materials in Raman spectra. This band exhibits dispersion, and the slope of the dispersion curve has been estimated to be  $\sim 90\text{ cm}^{-1}/\text{eV}$  [87, 90]. The D band (D, here, is generally referred to as defects), seen at around  $1350\text{ cm}^{-1}$ , is again a second-order process, but it arises due to inelastic scattering of the excited electron by a phonon followed

by elastic scattering by a defect. This band is an outcome of the so-called ‘breathing of carbon hexagons’. Similar to G’ band, the D band also shows dispersive nature with the slope of dispersion curve  $\sim 50 \text{ cm}^{-1}/\text{eV}$  [87, 90]. It is important to note here that the G’ band, being the overtone of the D band, is twice as dispersive as the D band. Sometimes other bands associated with the double resonance mechanism in which a defect instead of a second phonon is responsible for the conservation of momentum are also observed, such as D’ band at  $\sim 1620 \text{ cm}^{-1}$  and D’’ band at  $\sim 1100 \text{ cm}^{-1}$  [91].

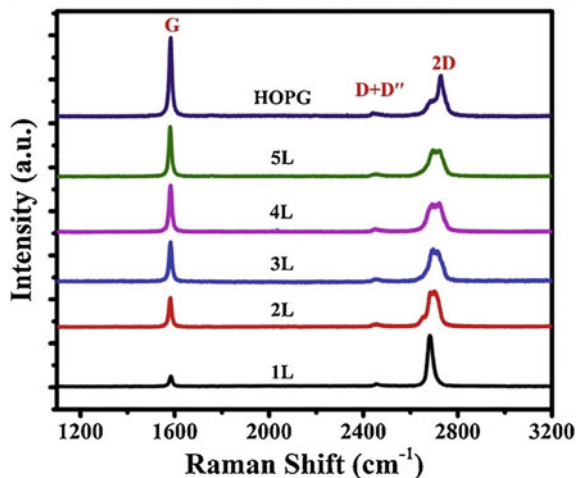
Y. You et al. studied the correlation between the intensity of D band and crystal orientation (edge chirality) of graphene [92]. Their study revealed that for the zigzag edge of graphene, the D band is either absent or is of very low intensity, while the armchair structure produces a much intense D band. G band has also been studied for determining the orientation of the graphene sheet [24]. The D band intensity, being a more prominent Raman signature of defects than the G’ band, is a measure of the number of defects in the graphene crystal. The nature of defects also plays a significant role in altering the Raman spectrum of graphene. A detailed study in this regard was performed by A. Eckmann et al. [22]. The study discloses the dependence of the intensity ratio of D band and D’ band ( $I_D/I_{D'}$ ) on the type of defects such as a change in hybridization at some locations to  $sp^3$  (instead of  $sp^2$ ) and the creation of vacancies. In the study, the intensity ratio was found to be  $\sim 13$  for  $sp^3$  defects and  $\sim 7$  for vacancy type defects. A more careful study on the sub-bands of the D band for suspended graphene was done by Z. Luo et al. [93]. They mainly focused on whether the scattering first takes place through a phonon or a defect. The research demonstrates that the two processes give rise to two D sub-bands.

A relative intensity, taking the intensity of the G band ( $I_G$ ) as a reference, rather than the intensity of the band under investigation, is generally estimated for quantitative and qualitative analysis of defects, doping, and the number of graphene layers in the system. G.S. Papanai et al. studied the intensity of the G’ band as a function of the number of graphene layers on Si/SiO<sub>2</sub> substrate [94]. The G’ band of an SLG consists of one Lorentzian peak of high intensity ( $I_{G'}/I_G = 24$ ) resulting from one double resonance process. For two layers stacked in the Bernal AB pattern, the system becomes more complex, and four double resonance processes take place, due to which the G’ band becomes a superposition of four Lorentzian peaks. The intensity of the G’ band compared to the G band is significantly reduced ( $I_{G'}/I_G \leq 1$ ). Scattering possibilities keep increasing with the number of layers, and the G’ band becomes a combination of multiple Lorentzian peaks, each representing a scattering phenomenon. The relative intensity ( $I_{G'}/I_G$ ) also decreases, which can be estimated to calculate the number of graphene layers. Figure 7 shows the Raman spectra for 1–5 graphene layers and HOPG.

The positions of G and G’ bands change with doping because of coupling between electron and phonon and are, therefore, studied to estimate the doping concentration in graphene [95]. The G band shifts towards higher values of Raman shift, and its width is also reduced with increasing dopant concentration. However, the dependency of the G’ band is different for electron concentration and hole concentration. The



**Fig. 7** Raman spectra for different numbers of graphene layers on Si/SiO<sub>2</sub> substrate [94]



position of the G' band shifts upwards with increasing hole concentration while in the reverse direction for increasing electron concentration [23].

The temperature change significantly affects the position of the G band. I. Calizo and his group calculated the temperature coefficient of the G band peak position for SLG and two-layer graphene [26]. For SLG, the value was measured to be  $-1.62 \times 10^{-2} \text{ cm}^{-1}/^\circ\text{C}$ , while for the two layers, it was found to be  $-1.54 \times 10^{-2} \text{ cm}^{-1}/^\circ\text{C}$ . The negative value indicates a blue shift in the scattering frequency when the temperature is increased. Various other parameters such as pressure, [25] strain, [96] etc. have also been found to be affecting the Raman spectrum of graphene, making it one of the most valuable tools to study graphene and related carbon materials.

## 4.2 Selected Area Electron Diffraction (SAED)

Diffraction is simply a change in a wave's path around the corners of and reaching in geometrical shadow regions of an obstacle. The electrons, behaving as waves, are diffracted by atoms in a crystal, and a pattern of diffraction maxima and minima emerges. This pattern, obtained for a small area, is called SAED and has long been used to study the crystallinity and crystal structure of materials. It is another valuable tool to analyze the quality of synthesized graphene. First of all, the technique is used for assessing the crystallinity of graphene sheets by visual analysis of the electron diffraction pattern. Distinct and sharp spots arranged in a hexagonal pattern with six-fold symmetry indicate the crystalline nature of graphene [97]. Furthermore, by finding the intensity ratios of various spots corresponding to different planes, the number of graphene layers present in the material can be estimated. The intensity ratio of (1–210) and (1–100) points (Miller-Bravais indices) is measured, and a value of less than unity indicates monolayer graphene. On the other hand, research groups

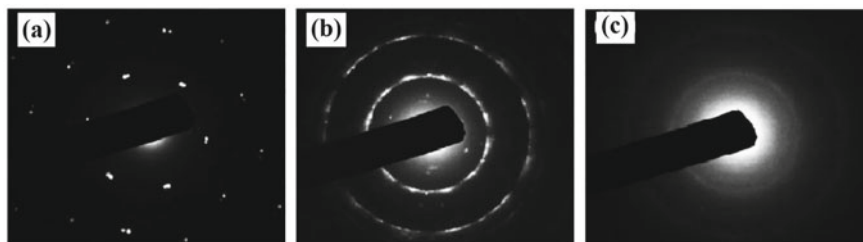


**Fig. 8** SAED patterns attributed to **a** Graphene (with some overlapping/folding/rotational stacking), **b** MLG with some amorphous carbon, and **c** only amorphous carbon [102]

have reported different values for MLG, but a value close to 2 for bilayer and 4 for trilayer Bernal AB stacking is generally observed [98–100]. All these groups have also confirmed the results with Raman spectroscopy.

Sharp concentric rings appear, in general, for polycrystalline materials with randomly oriented crystallites. Similarly, a random orientation of sheets in MLG (instead of Bernal AB structure) results in a sharp diffraction pattern with rings and some intense points on the rings [101]. Similar multiple ring patterns with maxima points can also appear due to the presence of amorphous carbon along with graphene sheets, as can be seen in Fig. 8b. In contrast, only the halo ring pattern similar to Fig. 8c infers the absence of crystallinity and, thus, of graphene (only amorphous carbon is present) [102]. MLG, with slight misalignment between layers, produces a cometic aberration-like pattern (Fig. 8a) instead of sharp points [103].

It is necessary to point out here that the electron beam is focused in a small area, and thus, the results obtained give information only on that particular area of the material. For thorough investigation, data should be obtained from different regions of the sample separated by a fixed distance through SAED mapping [97, 99]. Some researchers have proposed more sophisticated but faster methods to circumvent this issue for large area sheets [104].

### 4.3 Microscopic Techniques

Non-microscopic techniques for the characterization of graphene provide data based on the material's properties, but a visual perspective makes an entirely different impact on the understanding of a material. Optical microscopy is one of the oldest in this category and is also employed for studying graphene in the micro regime, but the information it reveals is very limited [105]. Transmission electron microscopy (TEM), especially with high resolution (HRTEM), is a powerful tool to probe the materials in nano and even sub-nano regimes. TEM is widely used to obtain information on surface topographies, growth patterns, and discontinuities. Sheet-level defects such as wrinkles, folds, kinks, rippling, and twists can be easily observed in TEM micrographs [27, 98, 103]. It is a highly recommended tool to study the potentially

preferred sites of the attachment [102, 106]. Information on a much deeper level, such as lattice defects, atomic planes, and interplanar spacing, can be obtained from the HRTEM [98]. It can also be utilized to measure the number of graphene layers by carefully examining high-resolution images of the edges [98, 99, 107].

Atomic force microscope (AFM) is different from other techniques because it uses a material cantilever tip, rather than electromagnetic (EM) waves or electrons, to probe the underlying material. It is another useful tool in the microscopy group to obtain crucial information about the synthesized graphene such as morphology, [108] imperfections, [109] functionalization, [110] mechanical, [29, 111] and electrical properties [28, 112]. The technique can also estimate the number of layers by measuring thickness, but results are not very reliable unless confirmed with other techniques. C.J. Shearer et al. conducted experiments to accurately measure the thickness of graphene with the help of AFM [105]. Apart from characterization, AFM can also be modified for controlled thermal reduction of GO to draw graphene patterns for the fabrication of electronic devices [113].

## 5 Applications

### 5.1 Electronics

One of the major problems that modern transistors face is power scaling with size. Dennard scaling law states that the power density of transistors remains the same, [114] but it no longer holds because of high leakage currents in devices with feature sizes less than 65 nm [115]. M.C. Lemme et al. first demonstrated the use of graphene as the channel material in field effect devices [116]. The power consumption was significantly reduced due to the high conductivity of graphene, and they were called graphene FETs or GFETs. A typical configuration of graphene channel field effect device is presented in Fig. 9. Graphene, being a zero bandgap semiconductor, causes turn-off issues in GFETs and makes them unsuitable for high-frequency applications, particularly for digital circuits [117]. Several proposed solutions such as electrical double layer gating, [118] uniaxially strained graphene, [119] graphene nanoribbons (GNRs), [120] high-k dielectrics, [121] and wrapped channel [122] have demonstrated potential. The performance was substantially enhanced, and up to  $10^7$   $I_{DS}$  ON/OFF ratio was achieved by using GNRs [120]. A novel configuration, MSIS-FET, was proposed by P. Li et al. with which they reported an even better ON/OFF ratio than GNRs [123].

Graphene has shown massive potential for light emitting diode (LED) applications. Graphene can be used for engineering various components such as electrodes and active material of the device. F. Withers et al. prepared van der Waals heterostructures using graphene, boron nitride, and metal chalcogenides to fabricate flexible LEDs with an extrinsic quantum efficiency of nearly 10% [124]. They also proposed

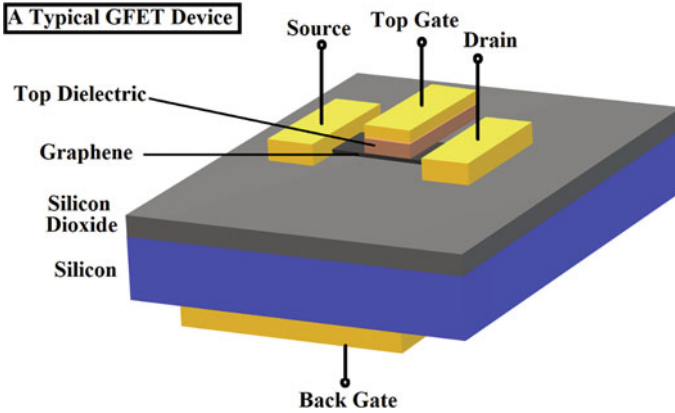


**Fig. 9** A typical graphene-based field effect device (GFET)

further improvements by introducing 2D layers of other chalcogenides. F. Rodríguez-Mas and his group introduced rGO in a previously explored structure for LED and reported better intensity with an unaffected output spectrum [125]. D. Yu et al. fabricated GaN micro-rod arrays on graphene films for flexible micro-LEDs emitting blue light [126]. Y.-X. Chen with his team prepared functionalized graphene quantum dots (QDs) from fullerenes and blended them with polyvinyl alcohol to form photoluminescent films that can transform ultraviolet LED into white [127]. Graphene is not only used for improving the existing LED devices but has also demonstrated the potential for novel all-graphene devices. X. Wang et al. demonstrated an all-graphene, wavelength-tunable LED device by using GO/rGO interface for producing light ranging from blue to red [128]. Graphene can also be used outside of the principal device to enhance its overall performance and stability [129].

## 5.2 Healthcare

The biocompatibility of graphene has been widely studied, [130, 131] which provides opportunities for its use in healthcare applications. Graphene has been explored for its potential in diagnostics, therapeutics, medicine, water purification, etc. It has provided technological advances in smart diagnostic tools for diseases and general health monitoring. A group led by W. Gao made a diagnosis and telemonitoring platform for COVID-19 [132]. A recent study shows that septicemia, which causes the immune system to damage its own tissues, can be diagnosed with the help of magnetic graphene-based micromotors [133]. Graphene-Based Transistors have also been applied to disease diagnosis [134]. Graphene and its derivatives have exhibited potential for detection of common bacterial [135] and viral infections [136]. A large number of reports and reviews on graphene-based diagnostic tools for cancer

indicate its enormous potential for the sector. E.G. Afshar et al. have reviewed applications of graphene in the diagnosis and treatment of one of the most menacing cancers, Glioblastoma multiform [137]. R. Majidi and M. Nadafan theoretically studied the application of twin graphene to diagnose lung cancer by sensing exhaled gases in human breath with the help of density functional theory (DFT) [138]. An immune-sensor for detecting a biomarker (HER-2) for breast cancer diagnosis was developed by H. Nasrollahpour with his team [139]. The group exploited the electroluminescence property of rGO/chitosan nanocomposite for the purpose.

Graphene is not only suitable for diagnostics but also has properties that are desirable in various therapies. Graphene-based therapeutics is one of the hot topics in modern healthcare for superior quality products. Several medical scientists have proposed and demonstrated ideas for the evolution of existing approaches and innovation of techniques by exploiting the unmatched properties of graphene. Among other methods, graphene-based materials for photothermal therapy (PTT) have gained significant popularity for cancer treatment in the past decade. PTT involves the delivery of a photothermal agent to the infection site (infected cells) and its subsequent heating through exposure to the near-infrared (NIR) radiation resulting in the killing of infected cells (Fig. 10 represents the scheme). C.C. Barrera et al. studied the interaction between rGO/Fe<sub>3</sub>O<sub>4</sub> NC and cell membrane and the effects of PTT on the viability of the cells [140]. The results show an excellent potential of the material for PTT of cancer. Another iron oxide and rGO-based NC, Fe<sub>3</sub>O<sub>4</sub>/Au/rGO, was demonstrated by T.S. Ardakani et al. as an effective material for synergistic radio-/photo-therapy on the oral squamous carcinoma cell line [141]. The material was reported to have good biocompatibility for healthy cells while having cytotoxic effects on the infected ones. X. Jia et al. used a hybrid of rGO, Au nanostars, and lipid bilayer for PTT of pancreatic cancer [142]. The material also exhibits an improved targeting capability and hence a better efficacy. R. Lima-Sousa et al. demonstrated, for the first time, the use of injectable GO and rGO incorporated hydrogels for the treatment of breast cancer [143]. The system shows a chemo-photothermal effect to reduce the cancer cell viability to 34% with Doxorubicin:Ibuprofen. Another group reported functionalized rGO as drug loading platforms for targeted delivery of the drug, doxorubicin hydrochloride, and subsequent chemo-photothermal treatment [144]. Various other therapies utilizing graphene and derived materials, such as sonodynamic, [145] photodynamic, [146] magnetothermodynamic [147] have also been reported for tumor inhibition. Many researchers are exploring graphene-based scaffolds for regenerative medicines, which help enhance the repair process of damaged tissues, and have reported impressive results [148, 149].

### 5.3 Energy

The ever-growing energy demand requires continuous improvements in existing technologies for energy conversion and storage and the creation of new paths that can meet the needs of the future. Graphene has been extensively studied for solar energy

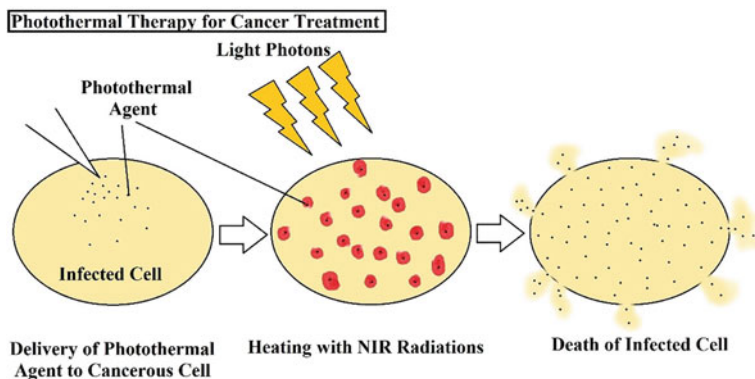


**Fig. 10** Step-by-step procedure of PTT for the treatment of cancer

conversion, irrespective of the type of device. However, substantial improvements in the performance of dye-sensitized solar cells (DSSCs) were observed with graphene introduced in photoanode or used at the counter electrode. One such device was fabricated and extensively characterized by F.W. Low et al. (shown in Fig. 11) [150]. They studied the effects of  $\text{TiO}_2$  content in rGO as photoanode material on the open-circuit voltage and short circuit current density of the device. S. Sun et al. also demonstrated the use of graphene/ $\text{TiO}_2$  composite for DSSC photoanodes and reported 59% enhanced efficiency compared to  $\text{TiO}_2$  photoanodes [151]. K. Basu et al. used graphene incorporated  $\text{SnO}_2/\text{TiO}_2$  composite as photoanode material and reported better efficiency and durability [152]. M.N. Mustafa and Y. Sulaiman prepared photoanode with graphene QDs decorated titania and identified the QDs as light scatters responsible for better performance [153]. The enhanced efficiency has been attributed to the enhanced dye loading due to increased surface area, which improves the carrier generation process. The addition of graphene also improves charge transfer by providing shorter paths to the electrode, reducing the carrier recombination rate. Pt has been the most widely used counter electrode by far; however, its high cost led many researchers to explore alternative options. Counter electrodes made by graphene ink spray deposited onto transparent conductive oxide (TCO) were reported by S. Casaluci et al. for large area DSSCs [154]. W.C. Oh et al. demonstrated the use of a rather complicated material, graphene composite with  $\text{Cu}_2\text{ZnNiSe}_4\text{-WO}_3$  nanorods, for efficient (even better than Pt) counter electrode material [155].

Apart from DSSCs, graphene has also exhibited potential for diverse applications in most other types of solar cells. For example, X. Miao et al. used SLG/n-Si for Schottky junction solar cells; [156]. J. Wu et al. made graphene transparent electrodes applied to organic solar cells; [157]. N.F. Ramali et al. inserted graphene passivation layer in perovskite solar cells; [158] graphene nanohills on silicon were illustrated for solar cell applications by M.A. Rehman et al. [159]. T. Lin and team used pristine and boron-doped graphene as the back electrode for CdTe solar cells [160].

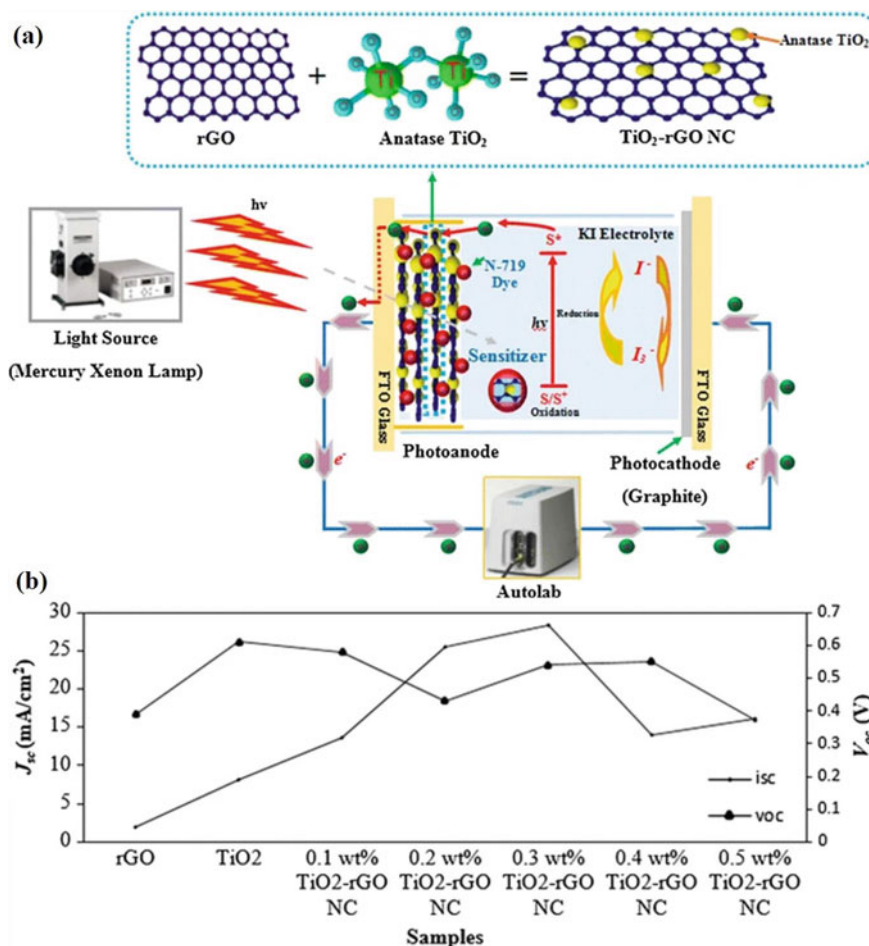


**Fig. 11** Schematic of the device fabricated by Low et al. (a) and results obtained from the device using different content of TiO<sub>2</sub> with graphene as photoanode material (b) [150]

The scope of energy generation, particularly through renewable sources, is limited unless a device can store it for later use. Batteries have long been used for energy storage and are the most prominent technology at present for the purpose. Amongst them, lithium-based batteries have been commercially available in the market for a long time. A large fraction of them uses graphite electrodes. As the technology is evolving, new materials are being explored to achieve higher charge storage capacities and longer cycle life. C. Wang et al. demonstrated the use of graphene paper as cathode for Li batteries [161]. N-doped graphene films have shown better Li-ion intercalation in an article by A.L. Mohana Reddy et al. [162]. J. Xiao et al. fabricated functionalized porous graphene structures for very high capacity (15,000 mAh/g) Li-air batteries [163]. Graphene-incorporated polymer-derived SiOC aerogels have

demonstrated stunning results as anode material for Li batteries [164]. X. Han et al. illustrated the use of core-shell structures (Si core, graphene shell) for Li-ion battery anodes [165]. Using a novel strategy with rGO/Ag-Li scaffolds as anode for Li-metal batteries was developed by T. Ma et al. [166]. A group from Zhejiang University led by C. Gao proposed a defect-free principle for high-performance Al-graphene batteries in 2017 [167]. He, leading another group, reported an exceptionally long cycle life of 250,000 for Al-graphene batteries later that same year [168].

Another prime requirement for an energy storage device is fast charging. Electrochemical capacitors, otherwise known as supercapacitors, are the most promising alternative to batteries with the inherent advantage of speedy charging. They offer high power density, but the energy density is low. Graphene-based electrodes have exhibited tremendous potential for supercapacitor applications because of graphene's high specific surface area. Supercapacitors made by RuO<sub>2</sub> modified rGO as anode and polyaniline modified rGO as cathode have been demonstrated by J. Zhang et al. [169]. L.T. Le et al. prepared supercapacitor electrodes by inkjet printing of GO on Ti and its subsequent thermal reduction [170]. Y. Fang et al. fabricated supercapacitor electrodes with functionalized graphene and demonstrated that the technology could bridge the gap between supercapacitor and battery with further optimizations [171]. H. Kim et al. proposed an all-graphene synergistic system for energy storage [172]. They also reported that the system works on both battery and supercapacitor mechanisms and thus creates a link between the two.

## 5.4 *Environmental Remediation*

Pollution, whether air, soil, water, or radiation, has caused much harm to the environment and human health. Scientists are looking for materials and devices that can be engineered for providing tools to reduce/eliminate pollution-causing agents. Many properties of graphene, such as corrosion resistance and mechanical and chemical stability, are ideal for environmental remediation applications. It has, therefore, been explored for removing pollutants, especially from water and air. Several reports have shown that graphene and derived materials are excellent for organic dye removal applications for wastewater treatment. H. Guo et al. reported GO/polyethylenimine (PEI) hydrogel for large-scale and efficient dye, Methylene Blue (MB) and Rhodamine B (RB), removal from wastewater [173]. They attributed the adsorption of dye to GO while PEI assisted the gelation process of GO. T. Jiao et al., however, synthesized rGO/Ag/PEI hydrogel via simultaneous reduction of GO and Ag<sup>+</sup> and suggested its application in catalytic degradation of MB and RB [174]. Y. Zhong and the group used dopamine GO composite decorated membrane to adsorb Congo Red and Basic Blue dyes [175]. They also demonstrated that treatment of membrane with a minute quantity of reducing agent (NaBH<sub>4</sub>) to reduce a small part of GO makes it useful for removal of small concentrations of methyl orange (MO), MB, RB, and 4-Nitrophenol. Photocatalytic dye (MB) degradation ability of Ag decorated rGO was exhibited by M. Ikram et al. [176]. Heavy metals in



water are another primary class of pollutants that are toxic to aquatic as well as non-aquatic life. T.A. Tabish et al. prepared highly porous graphene and demonstrated its application for efficiently removing MB and RB [177]. They further demonstrated the removal of oils (vegetable, engine, and pump oil), heavy metal (arsenic ion), and other harmful ions (fluoride and nitrate) from water. Many other groups also reported graphene-based techniques as promising candidates for heavy metal removal from wastewater. G. Zhao et al. prepared GO with the help of modified Hummer's method and displayed its application for sorption of Cd(II) and Co(II) from water [178]. K. Zhang et al. anchored TiO<sub>2</sub> nanoparticles on graphene sheets for effective reduction of Cr(VI) to Cr(III) [179]. A. Marjani et al. prepared GO dispersed in polyethersulfone membrane for degradation of MB and MO dyes and removal of heavy metal ions (Cu<sup>2+</sup>, Cd<sup>2+</sup>, and Zn<sup>2+</sup>) [180]. J. Zhang et al. studied, for the first time, the molecular interaction mechanism experimentally through single-molecule force spectroscopy and theoretically with DFT [181]. The study revealed critical aspects of molecular interactions that will help design graphene-based materials for wastewater treatment.

Though graphene has been extensively studied for the removal of water pollutants, it has also shown potential for removing contaminants from the air. V. Kumar et al. reviewed potential applications of graphene and related materials for adsorption and removal of volatile organic compounds [182]. W. Jung et al. fabricated a robust system by sandwiching a condenser between two layers of rGO filters to remove particulate matter from the air [183]. The group demonstrated the removal of both filterable and condensable particulate matter with the help of the fabricated system.

## 5.5 Sensing

Graphene, having a high surface-to-volume ratio, is an excellent material for sensing applications. Graphene has been applied to a range of sensors for physical parameters like pressure, temperature, strain, humidity, etc., and chemical species like gases, analytes, heavy metals, etc. Due to extraordinary mechanical and electrical properties, graphene has been studied extensively for pressure and strain sensors that are key to modern non-invasive techniques for health monitoring. Multiple innovative graphene-based wearable pressure and strain sensors were demonstrated by T.-L. Ren and associates for the purpose. In one report, they used tissue paper soaked in GO solution, which was later given thermal treatment to reduce GO for making pressure sensors for human motion detection [184]. Another report explains the use of Ag nanoparticles linked to graphene sheets over PDMS substrate for strain sensors that can monitor human motion [185]. In this work, the group used the laser scribing technique to reduce the GO. In another innovative work, an abrasive paper was used to make patterns on PDMS over which GO was deposited and subsequently reduced [186]. The rGO was then sandwiched by placing another layer of PDMS, forming a structure imitating the epidermis. The system was used to fabricate a wearable pressure sensor for human motion detection. A strain sensor for motion detection was made by dipping a polyester fabric in GO followed by thermal treatment to reduce

GO [187]. In a more recent work by T.-L. Ren and associates, a breathable graphene electronic skin, susceptible to strain and vibrations, and thus, useful for monitoring electrocardiogram, body motion, and respiration, was demonstrated [188]. A wearable pulse monitoring device with high sensitivity and long-range linear response graphene pressure sensor was reported by J. He et al. [189]. A graphene strain sensor for real-time pulse monitoring systems was explored by T. Yang et al. [190]. W. Liu et al. used wrinkled graphene for making piezoresistivity-based flexible, susceptible, and reliable pressure sensors [191]. Another class of graphene-based sensors, useful for healthcare applications, detect particular analytes from body fluids such as non-enzymatic glucose sensors [192, 193].

Z. Zheng and H. Wang performed first-principles calculations through DFT on doped and undoped graphene-based gas ( $\text{CO}_2$ ) sensors [194]. The results show a better performance with Al-doped than B-, N-, and P-doped graphene. Y. Seekaew and C. Wongchoosuk reported a novel  $\text{CO}_2$  sensor configuration utilizing electroluminescence with graphene film deposited over a patterned Ag electrode on a phosphor material [195]. G. Liu et al. fabricated a temperature sensor using rGO and demonstrated its use in robot skin for internet of things (IoT) [196]. B. Davaji et al. demonstrated the use of suspended SLG, deposited on  $\text{SiO}_2/\text{Si}$  substrate and SiN substrate for a resistance temperature sensor [197]. Devices formed on SiN substrates showed better performance. J. Yun et al. illustrated using graphene electrodes to build high-performance capacitive pressure sensors [198]. Graphene-based sensors for other physical quantities such as humidity, [199] refractive index, [200] magnetic field, [201] etc. have also been demonstrated.

## 5.6 Protective Coatings

Corrosion and biofouling are the major concerns for components used in marine applications and wastewater treatment. Graphene has displayed a great potential for protecting metals and alloys in corrosive conditions due to its hydrophobicity and impenetrability. F. Yu et al. demonstrated the use of the CVD process for graphene deposition on Al alloys for long-term corrosion protection [202]. A comparative study on GO and rGO based epoxy coatings for corrosion protection was performed by F.A. Ghauri et al. [203]. GO was found to be better protecting mild steel than rGO when exposed to a 3.5% NaCl solution. Y. Ye et al. reported better corrosion resistance with salinized aniline trimer functionalized graphene [204]. They reported that graphene forms an impermeable coating while salinized trianiline promotes self-healing of the underlying metal; thus, these synergistic effects provide better protection from the corrosive environment. S. Qiu et al. reported similar self-healing properties with polypyrrole intercalation in graphene [205].

Even with numerous reports of graphene providing protection from corrosive fluids, researchers have also shown that graphene coating can have degrading effects due to it being cathodic to most metals [206]. They have proposed that graphene inhibits corrosive solutions from reacting with underlying metal, but when a small

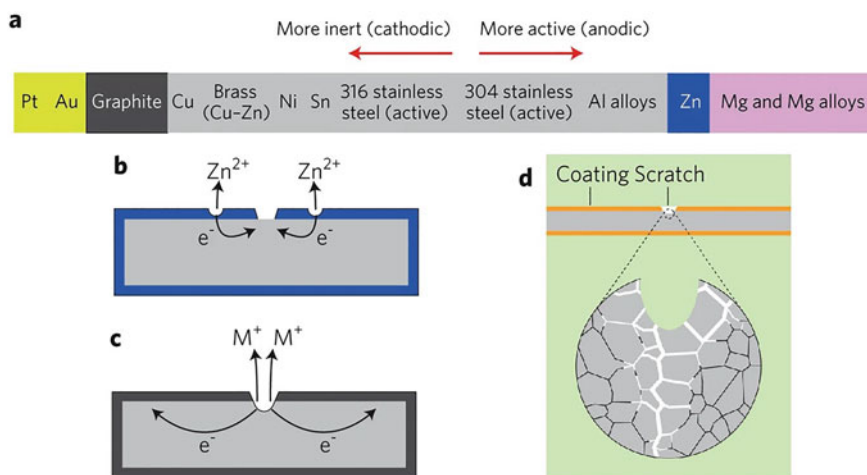


**Fig. 12** The chemistry of anticorrosion coatings: **a** the corrosion tendency of various metals and graphite (galvanic sequence), **b** anodic coating of Zn over steel, **c** cathodic coating promoting local oxidation, and **d** corrosion causing weakening of underlying metal/alloy by etching through grain boundaries. [206]

portion of the metal is exposed due to scratch or some other reason, graphene, being conductive, acts as the cathode and promotes localized oxidation (Fig. 12). The topic is debatable, and some material scientists have reported methods to circumvent this problem. X. Xu et al. demonstrated defect-free graphene coating on Cu(111) surface for durable protection from humid air [207].

Graphene/Si based antifouling coatings have shown vast potential, especially for maritime applications. H. Jin et al. proposed a novel graphene/Si rubber-based antifouling coatings and its working mechanism [208]. They proposed a mechanism inspired by sea animals having soft and flexible skin like dolphins due to which a dynamic surface is created, and they named it ‘harmonic motion effect’. They further reported, in another study, the effects of elastic modulus and color of the material on its antifouling properties [209]. M.S. Selim and the group also explored graphene/Si based materials for antifouling properties [210]. Antifouling coatings have also been proven advantageous for protecting sensors used in marine technology [211]. Multifunction coatings, such as antifouling coatings with anticorrosion [212] and antibacterial [213] effects, have also been proposed and tested.

## 6 Graphene Nanocomposites

Pristine graphene itself is a material with wonderful qualities and thus, has been studied for a range of applications and has been commercially employed in various industries. Other forms of graphene such as functionalized graphene, GNRs, GO,

and graphene NCs can have desired properties for several applications that pristine graphene cannot provide. Graphene has been utilized to make NC with many materials, including metals, metal oxides, metal sulfides, polymers, CNTs, epoxy, Mxenes, etc. Some of these NCs, especially their synthesis and applications, will be discussed in this section. It is crucial to point out that in some of these NCs, graphene will be used for reinforcement, while in others, graphene will be the matrix phase. Nevertheless, the properties are generally improved due to the synergistic effects of both phases.

## 6.1 Polymer-Graphene NCs

Graphene is hybridized with polymers to obtain materials having high mechanical strength, porosity, and thermal stability. Porous materials have a high specific surface area, one of the key requirements for electrochemical applications. X. Li et al. demonstrated the synthesis of highly porous polyaniline (PANI)/graphene NC through electropolymerization of PANI on graphene for electrochemical capacitors [214]. They reported up to 1209 F/gm specific capacitance and long cyclic stability with the synthesized materials. S. Fazli-Shokouhi et al. used in situ polymerization to prepare PANI-graphene NC, which demonstrated good anticorrosion and antifouling properties when incorporated in epoxy.[212] PANI- graphene NCs have also been used for EM interference mitigation [215]. In-situ polymerization, as presented schematically in Fig. 13, is one of the most appreciated methods for polymer-graphene NCs.

Poly-methyl methacrylate (PMMA) has been used for making composite materials with graphene through techniques such as in-situ emulsion polymerization, [216] precipitation polymerization, [217] solution blending method, [218] etc. The synthesized materials were characterized to find mechanical, thermal, and electrical properties [216] and dielectric and rheological properties [217]. Z. Zabihi et al.

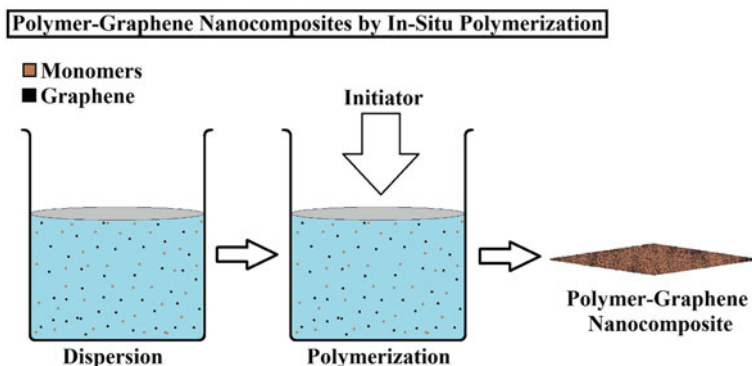


**Fig. 13** Steps involved in the in-situ polymerization process for the synthesis of polymer-graphene NCs

studied the interaction between the two components, graphene and PMMA, through theoretical simulations and their potential for detecting volatile organic compounds. [218].

Small quantities of graphene significantly improve the mechanical and thermal properties of polymers such as polyvinyl alcohol (PVA). The majority of researchers illustrated blending GO with PVA and then reduction of GO through a suitable method to obtain the desired rGO/PVA NC. X. Yuan reported improved tensile strength and thermal stability of PVA when 0.8% rGO was water blended into the polymer matrix [219]. X. Zhao et al. have reported 150% increased tensile strength and more than ten times enhanced Young's modulus with 1.8 vol % graphene addition via facial aqueous solution [220]. X. Wang et al. also reported improved mechanical and thermal properties of PVA with much smaller (0.1 and 0.3%) fractions of graphene [221]. They attributed strong interfacial interactions between the components to the improved tensile strength and restriction of motion of polymer chains by graphene sheets to the enhanced thermal stability. T. Zhou et al. obtained mechanically more robust and electrically conductive rGO/PVA NC with the help of a sodium hydrosulfite reducing agent [222].

Graphene has also been reported for making NC with polydopamine for strain sensor; [[223]] with poly(p-phenylenediamine) for detection of protein biomarkers; [224] with poly(isobutylene-co-isoprene) for barrier, dielectric, and sensing applications; [225] with polyimide [226] and poly(ethylene-co-methyl acrylate) [227] for EM interference shielding; with poly(butylene succinate) [228] and polyvinylbutyral [229] for improving thermal and mechanical properties; with poly(styrene sulfonate) [230] and poly vinyl pyrrolidone [231] for ascorbic acid sensing.

## 6.2 Metal-Graphene NCs

Metal-graphene NCs have shown potential in a large spectrum of applications ranging from electronics to biomedicine. Nickel, which also acts as a catalyst for the synthesis of graphene, can quickly form NCs with graphene via electrodeposition technique, which are widely employed in tribological applications [232–236]. It was reported by all these groups that incorporation of graphene in Ni increases hardness and, thus, increases wear resistance of the coating as compared to Ni coating. Surfactants, such as sodium dodecyl sulfate, were also used in deposition baths to further improve the synthesis process and hence the resultant properties of the coatings [232]. A. Jabbar et al. explored the effects of bath temperature in the range from 15°C to 60°C on deposited coatings and reported that moderate temperatures around 45°C are suitable for obtaining refined grain size and better microhardness [233]. A. Algul et al. extensively studied the effects of graphene content on wear mechanism [234]. A theoretical nanoindentation simulation study on Ni-graphene NCs was performed by S.-W. Chang et al. [237]. Their study reveals that an increasing number of graphene layers negatively impact the hardness but improve elastic deformability. The same group also performed atomistic simulations on Ni- and Cu-based graphene NCs to record

the effects of temperature and geometry on thermal interface conductance [238]. They reported that the effects are similar for both Ni and Cu. They also demonstrated that the SLG provides a high thermal interface conductance of  $\sim 500\text{MWm}^{-2}\text{K}^{-1}$ , which decreases to  $\sim 300\text{MWm}^{-2}\text{K}^{-1}$  for bilayer and  $150\text{MWm}^{-2}\text{K}^{-1}$  for trilayer. For more than three layers, the value ( $\sim 100\text{MWm}^{-2}\text{K}^{-1}$ ) becomes independent of the number of graphene layers.

Similar to Ni, Cu-graphene NCs have also been used for tribofilm formation. N. Khobragade et al. fabricated graphene-reinforced Cu NCs through the high-pressure torsion method and found that the synthesized NC with 10wt% graphene is twice as hard as pure copper [239]. S. Wang et al. also reported similar improvements in mechanical properties when graphene layers were directly deposited over Cu nanoparticles [240]. C.L.P. Pavithra et al. synthesized Cu-graphene NC foil via electrochemical route and reported  $\sim 250\text{Gpa}$  hardness, which is also close to the above-discussed results [241]. Not only tribological applications but Cu-graphene NCs have also been employed for sensing applications such as EC immune-sensors for detection of newcastle disease [242] and glucose sensor for food [243].

Noble metals such as Ag and Au have also been utilized to make NCs with graphene and have found applications in numerous areas. The synthesis protocols are quite similar but differ in the reduction methods applied for  $\text{Ag}^+/\text{Au}^{3+}$  ions and GO. In a typical procedure, an aqueous solution of silver/gold salt is mixed with an aqueous solution of GO, followed by simultaneous reduction of ions and GO [244–251]. Some researchers also reported sequential, instead of simultaneous, reduction of metal ions and GO [251]. The reducing agents may be chemical (e.g., sodium citrate, [244] hydrazine, [247, 251] sodium borohydride [246]) and biological (e.g., electrochemically active biofilms), [245, 249], or it can be done with other means such as electrochemistry [250] and exposure to ultraviolet radiations [248]. Bimetallic-graphene NCs have also been frequently reported in the literature. F. Tahernejad-Javazmi et al. studied rGO/FeNi<sub>3</sub> NCs applied to the detection of tert-butylhydroquinone in the presence of folic acid [252]. M.R. Vengatesan et al. used Ag–Cu/graphene NC for hybrid capacitance deionization application [253].

### 6.3 Metal Oxide-Graphene NCs

Metal oxides are one of the most crucial inorganic materials because they exhibit a range of properties with a distinct variation within each one. For example, metal oxides can have bandgaps such that some of them are narrow bandgap semiconductors or wide bandgap semiconductors, and others are insulators. NCs made by incorporating graphene into metal oxide matrix, or the other way around, offer novel properties desirable for many applications. Solvothermal/hydrothermal routes are generally employed for synthesizing NCs of graphene with metal oxides as well as sulfides. A typical procedure, as schematically represented in Fig. 14, involves the treatment of precursor material at high pressure and a temperature above the boiling

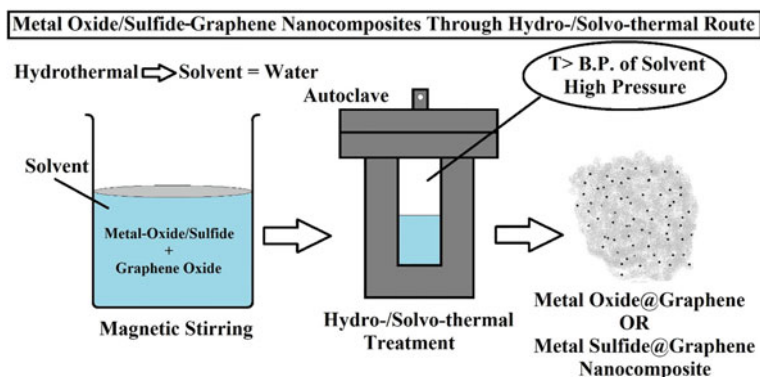


**Fig. 14** Solvo-/hydro-thermal route for the preparation of graphene-metal oxide/sulfide NCs

point (BP) of the solvent for 24 h. Titanium dioxide ( $\text{TiO}_2$ ), a wide bandgap material, makes NC with graphene, and the NC thus formed has been widely explored for solar cells, especially DSSCs, as discussed in section VI [151–153]. A group led by Y.-J. Xu has studied the photocatalytic applications of  $\text{TiO}_2$ /graphene NC for the degradation of volatile aromatic compounds [254] and oxidation of alcohols [255]. Both these reports compared the photocatalytic activity of  $\text{TiO}_2$ /graphene NC with  $\text{TiO}_2$ /CNT NC and reported better performance with the former.  $\text{TiO}_2$ /graphene NCs have also been employed for several other applications such as battery, [256] pseudo-capacitor, [257] and sensing [258]. Solvo-/hydro-thermal techniques are often used to synthesize graphene-metal oxide NCs, especially graphene- $\text{TiO}_2$  NCs. [254–256, 258].

Iron oxide, with its various oxidation states, has been reported to make NCs with graphene, which has found applications in multiple areas. S. Lee et al. prepared  $\text{Fe}_2\text{O}_3$ /graphene NC via a solventless route and demonstrated its use in detecting heavy metal ions ( $\text{Zn}^{2+}$ ,  $\text{Pb}^{2+}$ , and  $\text{Cd}^{2+}$ ) [259]. H. Su et al. prepared  $\text{FeO}_x$ /GO NC using the co-precipitation method and demonstrated its use for highly efficient arsenic removal [260]. Y. Yuan et al. employed a hydrothermal method with hydrazine to reduce GO and prepare  $\text{Fe}_2\text{O}_3$ /graphene NC applied as a catalyst for the thermal decomposition of  $\text{NH}_4\text{ClO}_4$  [261]. Numerous research papers on iron oxide/graphene NC as anode material for batteries stipulate its potential for energy storage devices. L. Xiao et al. used direct self-assembly of iron oxide and GO followed by hydrothermal treatment to reduce GO to synthesize  $\text{Fe}_2\text{O}_3$ /rGO NC [262]. They demonstrated its use as anode material in lithium-ion batteries with superior performance. W. Jiang et al. reported preparing a novel  $\text{FeO}_x$ /graphene NC through a solid-state method and exhibited its use as anode material for nickel–iron batteries [263]. They ball-milled ferrous oxalate dihydrate, GO, and glucose (reducing agent) followed by a series of heating processes to obtain the final product. H. Ren et al. used a simple hydrothermal method for obtaining Mn-doped  $\text{Fe}_3\text{O}_4$ /graphene NC

for Na-ion batteries [264].  $\text{Fe}_3\text{O}_4$ /graphene NCs have also attracted attention for mitigating EM pollution [265, 266].

Copper oxide/graphene NCs for Li-ion batteries have also been well documented in the literature. B. Wang et al. prepared CuO/graphene NC through simple stirring and centrifugation processes [267]. They reported much enhanced cyclic performance with the NC compared to anodes made by using only CuO nanoparticles. A.K. Rai also reported a significant enhancement in the cyclic performance of CuO/graphene NC for Li-ion batteries [268]. They, however, used short time spex-milling for obtaining the desired composite materials. L.L. Perreault et al. prepared graphene-wrapped Cu-Ni oxide nanoparticles with remarkable performance as Li-ion battery anode [269]. The group spray-dried the oxide nanoparticles and graphene mixture to form the NC. The use of CuO/graphene NC as an interfacial layer of metal/interlayer/semiconductor junction diode was demonstrated by Z. Orhan et al. [270]. They also studied gamma radiation resistance properties of the layer to demonstrate the device's ability to work in a radiation-rich environment. L. Luo et al. discussed CuO/graphene NC for non-enzymatic highly sensitive glucose sensor applications [271].

Several materials engineers have exploited ZnO/graphene NCs for photocatalysis, [272, 273] sensing, [274, 275] solar energy conversion, [276] and pollution mitigation[[277]] applications. Preparation methods and thus the synthesized NCs differ in properties, with the most common route again being the solvothermal method [273, 277]. Other methods that have also been explored oftentimes include combinations of stirring, ultrasonication, and centrifugation techniques; [272, 274] ball milling; [273] and in-situ reduction of zinc acetate and GO [275, 276]. Tin oxide ( $\text{SnO}_2$ ) is also hybridized with graphene to form NC materials that have found applications in many interesting areas. Na/Li-ion batteries have seen much advancement due to the synergistic effects of graphene and tin oxide on the anode [278, 279]. D. Zhang et al. developed highly sensitive humidity sensors using  $\text{SnO}_2$ /graphene NCs [279].

## 6.4 Metal Sulfide-Graphene NCs

Metal sulfides have been materials of interest for the scientific community working in diverse areas, from energy to biomedicine. Some of them, such as  $\text{MoS}_2$  and  $\text{SnS}$ , have layered structures similar to graphite, making them suitable for high surface area applications such as energy storage. The addition of graphene to these metal sulfides allowed researchers to push the performance limits in these research areas.

Graphene NCs with tin sulfides ( $\text{SnS}$  and  $\text{SnS}_2$ ) have been researched for multiple applications, energy conversion and storage remain the dominant ones. M. Zhang et al. introduced a novel solvothermal technique to synthesize  $\text{SnS}_x$ /graphene NC and demonstrated its application as anode material for Li-ion batteries [280]. Researchers have been following the route with few or no modifications to synthesize metal sulfide/graphene NCs. T. Ma and the team also used the solvothermal method to prepare  $\text{SnS}$ /graphene NC, which was later covered by N-doped carbon coating [281].



They demonstrated the use of this material to make anodes for Li-ion batteries. J. Shi et al. used graphene sheets hybridized with N, S co-doped carbon-coated SnS nanoflakes, synthesized again via solvothermal route, for Na-ion battery applications [282]. B. Yang et al. used solvothermal technique for the preparation of SnS/graphene NC applied to counter electrodes for DSSCs, replacing the commonly employed Pt electrode [283]. Another group used the hydrothermal route for the fabrication of flexible SnS<sub>2</sub>/graphene sensors for NO<sub>2</sub> detection [284]. J. Johny et al. made SnS/graphene NCs for solar energy conversion and electrochemical applications, but they followed a rather different synthesis protocol. The procedure involved spraying a mixture of SnS and GO onto moderately (120 and 250 °C) heated substrates to obtain the desired material [285].

Cadmium sulfide (CdS), with its various forms (films, nanoparticles, etc.), is a popular material for solar cell applications [286]. When blended with conducting graphene, CdS can also be employed for scores of other applications. Hydrogen production is one such sector where CdS/graphene NCs have been extensively studied [287–289]. A group led by T. Peng used GO, cadmium acetate, and dimethyl sulfoxide as precursor materials which were given solvothermal treatment for CdS/rGO NC preparation [287]. The same group also reported using unreduced GO to form NC with CdS and its application in H<sub>2</sub> storage [288]. In this work, they just stirred the GO and cadmium acetate mixture and added Na<sub>2</sub>S dropwise, skipping the thermal treatment step with the autoclave. S. Hammadi et al. used 7–8 layer graphene (purchased), cadmium sulfate, and thiourea as precursors for NC synthesis [289]. They performed experiments to display its potential for solar cells in addition to H<sub>2</sub> production applications. CdS/graphene NC has also exhibited potential for photoelectrochemical sensing applications in a report by L. Ge et al. [290]. They used an entirely different approach for NC synthesis directly onto an indium tin oxide (ITO) coated glass with the help of a direct-laser writing technique. The same article also demonstrated the fabrication of sensing devices with PbS/graphene NC through a similar approach. Other researchers have also investigated PbS/graphene NCs for sensing applications [291].

Cobalt sulfide (CoS)/graphene NCs have found applications in supercapacitors [292–294] and, like other metal-sulfide/graphene NCs, are generally prepared by solvothermal route [292, 293, 295]. R. Ramachandran et al., however, demonstrated the use of oil bath technique to synthesize the material [294]. G. Huang et al. described their cobalt sulfide phase as a mixture of CoS, CoS<sub>2</sub>, and Co<sub>9</sub>S<sub>8</sub> and demonstrated the use of NC thus formed for Li storage with excellent cyclic performance [295]. Graphene NCs with several other metal sulfides have also been investigated, but the list is long, and thus we will restrict this discussion by mentioning them with a few of their applications. MoS<sub>2</sub>, for instance, has been studied for EM pollution removal, [296] hydrogen evolution reaction, [297] desalination, [298] etc. Copper sulfide (CuS)/graphene NCs have been explored for hydrazine and hydrogen peroxide sensors, [299] biosensor to detect trichloroacetic acid [300] etc. Various reports on the supercapacitor application of nickel sulfide (NiS)/graphene NC can be found in the literature [301, 302]. Sulfides of tungsten (WS<sub>2</sub>) [303] and vanadium (VS<sub>2</sub>) [304]

have been investigated for sensing dihydroxybenzene isomers (catechol, resorcinol, hydroquinone) and Li-ion batteries, respectively.

## 7 Summary and Future Prospects

In this chapter, graphene and its nanocomposites with several crucial organic and inorganic materials have been discussed. Researchers from across the globe unanimously believe that graphene is a material of unmatched properties and, therefore, has a bright future. This chapter is designed to encourage this faith to further add to what researchers have achieved in the past two decades with graphene. The challenges that current technologies face for the scaled-up production of graphene and the currently available options to circumvent these issues have been explored. The discussion has an emphasis on the liquid phase exfoliation (LPE) process as it is a simple and one of the most promising techniques for cost-effective production of commercial-grade graphene in larger quantities.

Characterization tools are required for the quality assessment of graphene. Few of them, which reveal critical information, have been discussed in the chapter. Basics of Raman spectroscopy and various aspects of it, when implemented for characterization of graphene, have been critically discoursed. The origin of different bands appearing in the Raman spectrum of graphene, their broadening and shifting due to structural changes introduced by imperfections have been discussed. SAED was introduced, within the scope of graphene, for information on the crystal structure and stacking of layers. A brief discussion of microscopic tools such as TEM and AFM has also been presented.

The remarkable properties of graphene made curious minds wonder about their exploitation in real-world applications. In this chapter, applications of graphene are reviewed in electronics, healthcare, energy, environmental remediation, sensing, and protective coating sectors. Graphene nanocomposites are generally prepared to optimize properties for application-specific requirements. For example, graphene NCs with metals have excellent tribological properties, while NCs with metal oxides and sulfides have shown much potential for energy storage devices, especially batteries and supercapacitors. A discussion on the nanocomposites of graphene with polymers, metals, metal-oxides, and sulfides has been included in the chapter.

## References

1. Yazyev OV (2016) Theory of magnetism in graphitic materials. In: Esquinazi P (eds) Basic physics of functionalized graphite. Springer Series in Materials Science, Springer, Cham. 244
2. Popov IA, Bozhenko KV, Boldyrev AI (2012) Is Graphene Aromatic? *Nano Res* 5(2):117–123
3. Wallace PR (1947) The Band Theory of Graphite. *Phys Rev* 71:622
4. Novoselov KS, Geim AK, Morozov SV, Jiang D, Zhang Y, Dubonos SV, Grigorieva IV, Firsov AA (2004) Electric field effect in atomically thin carbon films. *Science* 306:666

5. E. Reich, Nobel prize committee under fire. *Nature* (2010)
6. Kundhikanjana W, Lai K, Wang H, Dai H, Kelly MA, Shen Z (2009) Hierarchy of electronic properties of chemically derived and pristine graphene probed by microwave imaging. *Nano Lett* 9(11):3762–3765
7. Ghosh S, Nika DL, Pokatilov EP, Balandin AA (2009) Heat conduction in graphene: experimental study and theoretical interpretation. *New J Phys* 11:095012
8. Ovid'ko IA (2013) Mechanical properties of graphene. *Rev Adv Mater Sci* 34, 1–11
9. Bolotin KI, Sikes KJ, Jiang Z, Klima M, Fudenberg G, Hone J, Kim P, Stormer HL (2008) Ultrahigh electron mobility in suspended graphene. *Solid State Commun* 146:351–355
10. McAllister MJ, Li JL, Adamson DH, Schniepp HC, Abdala AA, Liu J, Herrera-Alonso M, Milius DL, Car R, Prud'homme RK, Aksay IA (2007) Single sheet functionalized graphene by oxidation and thermal expansion of graphite. *Chem Mater* 19:4396–4404
11. Lemme MC (2009) Current status of graphene transistors. *Solid State Phenom* 156–158:499–509
12. Atalaya J, Isacson A, Kinaret JM (2008) Continuum elastic modeling of graphene resonators. *Nano Lett* 8(12):4196–4200
13. Wei Z, Chen Y, Dames C (2013) Negative correlation between in-plane bonding strength and cross-plane thermal conductivity in a model layered material. *Appl Phys Lett* 102:011901
14. Pop E, Varshney V, Roy AK (2012) Thermal properties of graphene: Fundamentals and applications. *MRS Bull* 37:1273–1281
15. Rho H, Jang YS, Bae H, Cha A-N, Lee SH, Ha J-S (2021) Fanless, porous graphene-copper composite heat sink for micro devices. *Sci Rep* 11:17607
16. Pirruccio G, Moreno LM, Lozano G, Rivas JG (2013) Coherent and broadband enhanced optical absorption in graphene. *ACS Nano* 7(6):4810–4817
17. Pang S, Hernandez Y, Feng X, Müllen K (2011) Graphene as transparent electrode material for organic electronics. *Adv Mater* 23(25):2779–2795
18. Tetlow H, Posthuma de Boer J, Ford IJ, Vvedensky DD, Coraux J, Kantorovich L (2014) Growth of epitaxial graphene: Theory and experiment. *Phys Rep* 542:195–295
19. Muñoz R, Gómez-Aleixandre C (2013) Review of CVD synthesis of graphene. *Chem Vap Deposition* 19:297–322
20. Cai M, Thorpe D, Adamson DH, Schniepp HC (2012) Methods of graphite exfoliation. *J Mater Chem* 22:24992–25002
21. Niilisk A, Kozlova J, Alles H, Aarik J, Sammelselg V (2016) Raman characterization of stacking in multi-layer graphene grown on Ni. *Carbon* 98:658–665
22. Eckmann A, Felten A, Mishchenko A, Britnell L, Ralph Krupke, Novoselov KS, Casiraghi C (2012) Probing the nature of defects in graphene by raman spectroscopy. *Nano Lett.* 12, 3925–3930
23. Beams R, Cancado LG, Novotny L (2015) Raman characterization of defects and dopants in graphene. *J Phys: Condens Matter* 27, 083002
24. Cong C, Yu T, Wang H (2010) Raman study on the G mode of graphene for determination of edge orientation. *ACS Nano* 4(6):3175–3180
25. Proctor JE, Gregoryanz E, Novoselov KS, Lotya M, Coleman JN, Halsall MP (2009) High-pressure Raman spectroscopy of graphene. *Phys Rev B* 80:073408
26. Calizo I, Balandin AA, Bao W, Miao F, Lau CN (2007) Temperature dependence of the raman spectra of graphene and graphene multilayers. *Nano Lett* 7(9):2645–2649
27. Suh YJ, Park SY, Kim MJ (2009) High resolution TEM and electron diffraction study of graphene layers. *Microsc Microanal* 15(S2):1168–1169
28. Yu Z, Song A, Sun L, Li Y, Gao L, Peng H, Ma T, Liu Z, Luo J (2020) Understanding interlayer contact conductance in twisted bilayer graphene. *Small* 16:1902844
29. Teklu A, Barry C, Palumbo M, Weiwadel C, Kuthirummal N, Flagg J (2019) Mechanical characterization of reduced graphene oxide using AFM. *Adv Condens Matter Phys* 2019:8713965
30. Collins R (30 Dec, 2021) Graphene market & 2D materials assessment 2021–2031, IDTechEx, <https://www.idtechex.com/en/research-report/graphene-market-and-2d-materials-assessment-2021-2031/789>

31. Hybrid Solutions Graphene, Turtle Wax, (30 Dec, 2021) <https://www.turtlewax.com/collections/hybrid-solutions-graphene>
32. Graphene 360+, Head, (30 Dec, 2021) <https://www.head.com/en/sports/tennis/technology/graphene360plus>
33. G-Series, inov-8, (30 Dec, 2021) <https://www.inov-8.com/row/g-series>
34. G1 wonders, (30 Dec, 2021) <https://g1wonders.com/shop/>
35. Graphene XT, (30 Dec, 2021) <https://www.graphene-xt.com/en/>
36. Badami D (1962) Graphitization of  $\alpha$ -Silicon carbide. *Nature* 193:569–570
37. Norimatsu W, Kusunoki M (2014) Growth of graphene from SiC{0001} surfaces and its mechanisms. *Semicond Sci Technol* 29:064009
38. Rohbeck N, Xiao P (2014) Effects of thermal treatment on the mechanical integrity of silicon carbide in HTR fuel up to 2200°C. *J Nucl Mater* 451:168–178
39. Badami DV (1965) X-Ray studies of graphite formed by decomposing silicon carbide. *Carbon* 3(1):53–57
40. Berger C, Song Z, Li T, Li X, Ogbazghi AY, Feng R, Dai Z, Marchenkov AN, Conrad EH, First PN, de Heer WA (2004) Ultrathin epitaxial graphite: 2D electron gas properties and a route toward graphene-based nanoelectronics. *J Phys Chem B* 108(52):19912–19916
41. Wofford JM, Oliveira MH Jr, Schumann T, Jenichen B, Ramsteiner M, Jahn U, Fölsch S, Lopes JMJ, Riechert H (2014) Molecular beam epitaxy of graphene on ultra-smooth nickel: growth mode and substrate interactions. *New J Phys* 16:093055
42. Zheng R, Xu Z, Khanaki A, Tian H, Zuo Z, Zheng J-G, Liu J (2017) Low-temperature growth of graphene on iron substrate by molecular beam epitaxy. *Thin Solid Films* 627:39–43
43. Garcia JM, He R, Jiang MP, Yan J, Pinczuk A, Zuev YM, Kim KS, Kim P, Baldwin K, West KW, Pfeiffer LN (2010) Multilayer graphene films grown by molecular beam deposition. *Solid State Commun* 150:809–811
44. Cheng TS, Davies A, Summerfield A, Cho YJ, Cebula I, Hill RJA, Mellor CJ, Khlobystov AN, Taniguchi T, Watanabe K, Beton PH, Foxon CT, Eaves L, Novikova SV (2016) High temperature MBE of graphene on sapphire and hexagonal boron nitride flakes on sapphire. *J Vac Sci Technol B* 34:02L101
45. Dabrowski J, Lippert G, Avila J, Baringhaus J, Colambo I, Dedkov YuS, Herziger F, Lupina G, Maultzsch J, Schaffus T, Schroeder T, Kot M, Tegenkamp C, Vignaud D, Asensio M-C (2016) Understanding the growth mechanism of graphene on Ge/Si(001) surfaces. *Sci Rep* 6:31639
46. Dillemans L, Tran T, Bhuiyan NK, Smets T, Menghini M, Lieten R, Seo JW, Locquet J-P (2011) Epitaxial growth of V2O3 on Al2O3 by reactive MBE. *MRS Online Proc Libr* 1292:61–66
47. Schumann T, Lopes JMJ, Wofford JM, Oliveira MH Jr, Dubslaff M, Hanke M, Jahn U, Geelhaar L, Riechert H (2015) The impact of substrate selection for the controlled growth of graphene by molecular beam epitaxy. *J Cryst Growth* 425:274–278
48. Hernández-Rodríguez I, García JM, Martín-Gago JA, de Andrés PL, Méndez J (2015) Graphene growth on Pt(111) and Au(111) using a MBE carbon solid-source. *Diam Relat Mater* 57:58–62
49. Wang M, Luo D, Wang B, Ruoff RS (2021) Synthesis of Large-Area Single-Crystal Graphene. *Trends Chem.* 3(1):15–33
50. Cushing GW, Johaneck V, Navin JK, Harrison I (2015) Graphene Growth on Pt(111) by ethylene chemical vapor deposition at surface temperatures near 1000 K. *J Phys Chem C* 119(9):4759–4768
51. Chung WR, Zhao Y, Oye M, Nguyen C (2011) Graphene synthesis by thermal-CVD method. In: 2011 11th IEEE International Conference on Nanotechnology, Portland Marriott, August 15–18
52. An H, Lee W-J, Jung J (2011) Graphene synthesis on Fe foil using thermal CVD. *Curr Appl Phys* 11:S81–S85
53. Land TA, Michely T, Behm RJ, Hemminger JC, Comsa G (1992) STM investigation of single layer graphite structures produced on Pt(111) by hydrocarbon decomposition. *Surf Sci* 264:261–270

54. Losurdo M, Giangregorio MM, Capezuto P, Bruno G (2011) Graphene CVD growth on copper and nickel: role of hydrogen in kinetics and structure. *Phys Chem Chem Phys* 13:20836–20843
55. McLellan RB (1969) The solubility of carbon in solid gold, copper, and silver. *Scr Mater* 3:389–392
56. Wood JD, Schmucker SW, Lyons AS, Pop E, Lyding JW (2011) Effects of polycrystalline Cu substrate on graphene growth by chemical vapor deposition. *Nano Lett* 11(11):4547–4554
57. Kalita G, Wakita K, Umeno M (2012) Low temperature growth of graphene film by microwave assisted surface wave plasma CVD for transparent electrode application. *RSC Adv* 2:2815–2820
58. Li N, Zhen Z, Zhang R, Xu Z, Zheng Z, He L (2021) Nucleation and growth dynamics of graphene grown by radio frequency plasma-enhanced chemical vapor deposition. *Sci Rep* 11:6007
59. Huet B, Raskin J-P, Snyder DW, Redwing JM (2020) Fundamental limitations in transferred CVD graphene caused by Cu catalyst surface morphology. *Carbon* 163:95–104
60. Chen Z, Qi Y, Chen X, Zhang Y, Liu Z (2019) Direct CVD growth of graphene on traditional glass: methods and mechanisms. *Adv Mater* 31:1803639
61. Niyogi S, Bekyarova E, Itkis ME, McWilliams JJ, Hamon MA, Haddon RC (2006) Solution properties of graphite and graphene. *J Am Chem Soc* 128:7720–7721
62. Yu P, Lowe SE, Simon GP, Zhong YL (2015) Electrochemical exfoliation of graphite and production of functional graphene. *Curr Opin Colloid Interface Sci* 20:329–338
63. Munuera JM, Paredes JI, Villar-Rodil S, Ayán-Varela M, Pagán A, Aznar-Cervantes SD, Cenis JL, Martínez-Alonso A, Tascón JMD (2015) High quality, low oxygen content and biocompatible graphene nanosheets obtained by anodic exfoliation of different graphite types. *Carbon* 94:729–739
64. Liu F, Wang C, Sui X, Riaz MA, Xu M, Wei L, Chen Y (2019) Synthesis of graphene materials by electrochemical exfoliation: Recent progress and future potential. *Carbon Energy* 1(2):173–199
65. Parvez K, Wu Z-S, Li R, Liu X, Graf R, Feng X, Müllen K (2014) Exfoliation of graphite into graphene in aqueous solutions of inorganic salts. *J Am Chem Soc* 136(16):6083–6091
66. Liu J, Poh CK, Zhan D, Lai L, Lim SH, Wang L, Liu X, Sahoo NG, Li C, Shen Z, Lin J (2013) Improved synthesis of graphene flakes from the multiple electrochemical exfoliation of graphite rod. *Nano Energy* 2:377–386
67. Achee TC, Sun W, Hope JT, Quitzau SG, Sweeney CB, Shah SA, Habib T, Green MJ (2018) High-yield scalable graphene nanosheet production from compressed graphite using electrochemical exfoliation. *Sci Rep* 8:14525
68. Hummers WS, Offeman RE (1958) Preparation of graphitic oxide. *J Am Chem Soc* 80:1339
69. Chua CK, Pumera M (2014) Chemical reduction of graphene oxide: a synthetic chemistry viewpoint. *Chem Soc Rev* 43:291–312
70. Sengupta I, Chakraborty S, Talukdar M, Pal S, Chakraborty S (2018) Thermal reduction of graphene oxide: How temperature influences purity. *J Mater Res* 33(23):4113–4122
71. Salunke BK, Kim BS (2016) Facile synthesis of graphene using a biological method. *RSC Adv* 6:17158–17162
72. Hamilton CE, Lomeda JR, Sun Z, Tour JM, Barron AR (2009) High-Yield organic dispersions of unfunctionalized graphene. *Nano Lett* 9(10):3460–3462
73. Hernandez Y, Nicolosi V, Lotya M, Blighe FM, Sun Z, De S, McGovern IT, Holland B, Byrne M, Gun'ko YK, Boland JJ, Niraj P, Duesberg G, Krishnamurthy S, Goodhue R, Hutchison J, Scardaci V, Ferrari AC, Coleman JN (2008) High-yield production of graphene by liquid-phase exfoliation of graphite. *Nat Nanotechnol.* 3, 563–568
74. Haar S, El Gemayel M, Shin Y, Melinte G, Squillaci MA, Ersen O, Casiraghi C, Ciesielski A, Samori P (2015) Enhancing the liquid-phase exfoliation of graphene in organic solvents upon addition of n-Octylbenzene. *Sci Rep* 5:16684
75. Bourlinos AB, Georgakilas V, Zboril R, Steriotis TA, Stubos AK (2009) Liquid-Phase exfoliation of graphite towards solubilized graphenes. *Small* 5(16):1841–1845

76. Telkhozhayeva M, Teblum E, Konar R, Girshevitz O, Perelshtein I, Aviv H, Tischler YR, Nessim GD (2021) Higher ultrasonic frequency liquid phase exfoliation leads to larger and monolayer to Few-Layer flakes of 2D layered materials. *Langmuir* 37(15):4504–4514
77. Monajjemi M (2017) Liquid-phase exfoliation (LPE) of graphite towards graphene: An ab initio study. *J Mol Liq* 230:461–472
78. Shin Y, Just-Baringo X, Boyes M, Panigrahi A, Zarattini M, Chen Y, Liu X, Morris G, Prestat E, Kostarelos K, Vranic S, Larrosa I, Casiraghi C (2021) Enhanced liquid phase exfoliation of graphene in water using an insoluble bis-pyrene stabiliser. *Faraday Discuss* 227:46–60
79. Li Z, Young RJ, Backes C, Zhao W, Zhang X, Zhukov AA, Tillotson E, Conlan AP, Ding F, Haigh SJ, Novoselov KS, Coleman JN (2020) Mechanisms of liquid-phase exfoliation for the production of graphene. *ACS Nano* 14(9):10976–10985
80. Yi M, Shen Z, Ma S, Zhang X (2012) A mixed-solvent strategy for facile and green preparation of graphene by liquid-phase exfoliation of graphite. *J Nanopart Res* 14:1003
81. Nuvoli D, Valentini L, Alzari V, Scognamillo S, Bon SB, Piccinini M, Illescas J, Mariani A (2011) High concentration few-layer graphene sheets obtained by liquid phase exfoliation of graphite in ionic liquid. *J Mater Chem* 21:3428–3431
82. Du W, Lu J, Sun P, Zhu Y, Jiang X (2013) Organic salt-assisted liquid-phase exfoliation of graphite to produce high-quality graphene. *Chem Phys Lett* 568–569:198–201
83. Qiu X, Bouchiat V, Colombet D, Ayela F (2019) Liquid-phase exfoliation of graphite into graphene nanosheets in a hydrocavitating ‘lab-on-a-chip.’ *RSC Adv* 9:3232–3238
84. Alinejad B, Mahmoodi K (2017) Synthesis of graphene nanoflakes by grinding natural graphite together with NaCl in a planetary ball mill. *Funct Mater Lett* 10:1750047
85. Lin T, Tang Y, Wang Y, Bi H, Liu Z, Huang F, Xie X, Jiang M (2013) Scotch tape-like exfoliation of graphite assisted with elemental sulfur and graphene–sulphur composites for high-performance lithium-sulfur batteries. *Energy Environ Sci* 6:1283
86. Alam MF, Khan MS, Uddin I, Khan SN, Ahmad I (2020) Exfoliation synthesis of graphene and optimization with alkali halides salts. *Surf Interfaces* 20:100548
87. Malard LM, Pimenta MA, Dresselhaus G, Dresselhaus MS (2009) Raman spectroscopy in graphene. *Phys Rep* 473(5–6):51–87
88. Dresselhaus MS, Dresselhaus G, Jorio A, Souza Filho AG, Saito R, Raman (2002) spectroscopy on isolated single wall carbon nanotubes. *Carbon* 40, 2043–2061
89. Artur CG, Miller R, Meyer M, Le Ru EC, Etchegoin PG (2012) Single-molecule SERS detection of C60. *Phys Chem Chem Phys* 14:3219–3225
90. Jorio A (2012) Raman spectroscopy in graphene-based systems: prototypes for nanoscience and nanometrology. *ISRN Nanomater.* 2012:234216
91. Jorio A, Dresselhaus MS, Saito R, Dresselhaus G (2011) Raman spectroscopy in graphene related systems. Wiley-VCH, Weinheim, Germany
92. You Y, Ni Z, Yu T, Shen Z (2008) Edge chirality determination of graphene by Raman spectroscopy. *Appl Phys Lett* 93:163112
93. Luo Z, Cong C, Zhang J, Xiong Q, Yu T (2012) The origin of sub-bands in the Raman D-band of graphene. *Carbon* 50:4252–4258
94. Papanai GS, Sharma I, Gupta BK (2020) Probing number of layers and quality assessment of mechanically exfoliated graphene via Raman fingerprint. *Mater Today Commun* 22:100795
95. Tang B, Guoxin H, Gao H (2010) Raman spectroscopic characterization of graphene. *Appl Spectrosc Rev* 45(5):369–407
96. Popov VN, Lambin P (2013) Theoretical Raman intensity of the G and 2D bands of strained graphene. *Carbon* 54:86–93
97. Geng D, Wu B, Guo Y, Huang L, Xue Y, Chen J, Yu G, Jiang L, Hu W, Liu Y (2012) Uniform hexagonal graphene flakes and films grown on liquid copper surface. *PNAS* 109:7992–7996
98. Shen Y, Lua AC (2013) A facile method for the large-scale continuous synthesis of graphene sheets using a novel catalyst. *Sci Rep* 3:3037
99. Li J, Ji H, Zhang X, Wang X, Jin Z, Wang D, Wan L-J (2014) Controllable atmospheric pressure growth of mono-layer, bi-layer and tri-layer graphene. *Chem Commun* 50:11012–11015

100. Luo B, Chen B, Wang A, Geng D, Xu J, Wang H, Zhang Z, Peng L, Xu Z, Yu G (2016) Chemical vapor deposition of bilayer graphene with layer-resolved growth through dynamic pressure control. *J. Mater. Chem. C* 4:7464–7471
101. Sengupta J, Das K, Nandi UN, Jacob C (2019) Substrate free synthesis of graphene nanoflakes by atmospheric pressure chemical vapour deposition using Ni powder as a catalyst. *Bull Mater Sci* 42:136
102. Cui T, Lv R, Huang Z-H, Zhu H, Jia Y, Chen S, Wang K, Wu D, Kang F (2012) Low-temperature synthesis of multilayer graphene/amorphous carbon hybrid films and their potential application in solar cells. *Nanoscale Res Lett* 7:453
103. Kaur A, Kaur J, Singh RC (2018) Green exfoliation of graphene nanosheets based on freezing induced volumetric expansion of carbonated water. *Mater Res Express* 5:085601
104. Zhao W, Xia B, Lin L, Xiao X, Liu P, Lin X, Peng H, Zhu Y, Yu R, Lei P, Wang J, Zhang L, Xu Y, Zhao M, Peng L, Li Q, Duan W, Liu Z, Fan S, Jiang K (2017) Low-energy transmission electron diffraction and imaging of large-area graphene. *Sci Adv* 3:e1603231
105. Shearer CJ, Slattery AD, Stapleton AJ, Shapter JG, Gibson CT (2016) Accurate thickness measurement of graphene. *Nanotechnology* 27:125704
106. Kim HJ, Lee S-M, Oh Y-S, Yang Y-H, Lim YS, Yoon DH, Lee C, Kim J-Y, Ruoff RS (2014) Unoxidized graphene/alumina nanocomposite: fracture- and wear-resistance effects of graphene on alumina matrix. *Sci Rep* 4:5176
107. Yan Z, Lin J, Peng Z, Sun Z, Zhu Y, Li L, Xiang C, Samuel EL, Kittrell C, Tour JM (2012) Toward the synthesis of wafer-scale single-crystal graphene on copper foils. *ACS Nano* 6(10):9110–9117
108. Haghighian N, Convertino D, Miseikis V, Bisio F, Morgante A, Coletti C, Canepa M, Cavalieri O (2018) Rippling of graphitic surfaces: a comparison between few-layer graphene and HOPG. *Phys Chem Chem Phys* 20:13322–13330
109. Prakash G, Capano MA, Bolen ML, Zemlyanov D, Reifengerger RG (2010) AFM study of ridges in few-layer epitaxial graphene grown on the carbon-face of 4H-SiC(000-1). *Carbon* 48(9):2383–2393
110. Ramphal IA, Hagerman ME (2019) Nanoscale morphology, tribology and electrical properties of polyaniline/graphene oxide/LAPONITE composites investigated using atomic force microscopy. *Nanoscale* 11:20876–20883
111. Lina L-Y, Kim D-E, Kim W-K, Jun S-C (2011) Friction and wear characteristics of multi-layer graphene films investigated by atomic force microscopy. *Surf Coat Technol* 205(20):4864–4869
112. Hauquier F, Alamarguy D, Viel P, Noël S, Filoramo A, Huc V, Houzé F, Palacin S (2012) Conductive-probe AFM characterization of graphene sheets bonded to gold surfaces. *Appl Surf Sci* 258(7):2920–2926
113. Wei Z, Wang D, Kim S, Kim S-Y, Hu Y, Yakes MK, Laracuento AR, Dai Z, Marder SR, Berger C, King WP, De Heer WA, Sheehan PE, Riedo E (2010) Nanoscale tunable reduction of graphene oxide for graphene electronics. *Science* 328(5984):1373–1376
114. Dennard RH, Gaensslen FH, Yu H, Rideout VL, Bassous E, LeBlanc AR (1974) Design of ion-implanted MOSFET's with very small physical dimensions. *IEEE J Solid-State Circuits* 9(5):256–268
115. Xue J, Li T, Deng Y, Yu Z (2010) Full-chip leakage analysis for 65nm CMOS technology and beyond. *Integration* 43:353–364
116. Lemme MC, Echtermeyer TJ, Baus M, Kurz H (2007) A graphene field-effect device. *IEEE Electron Device Lett* 28(4):282–284
117. Schwier F (2010) Graphene transistors. *Nat Nanotechnol* 5:487–496
118. Hayashi CK, Garmire DG, Yamauchi TJ, Torres CM, Ordóñez RC (2020) High on-off ratio graphene switch via electrical double layer gating. *IEEE Access* 8:92314–92321
119. Ni ZH, Yu T, Lu YH, Wang YY, Feng YP, Shen ZX (2008) Uniaxial strain on graphene: Raman spectroscopy study and bandgap opening. *ACS Nano* 2:2301–2305
120. Li X, Wang X, Zhang L, Lee S, Dai H (2008) Chemically derived, ultrasoft graphene nanoribbon semiconductors. *Science* 319:1229–1232

121. Robinson JA, LaBella M III, Trumbull KA, Weng X, Cavelero R, Daniels T, Hughes Z, Hollander M, Fanton M, Snyder D (2010) Epitaxial graphene materials integration: Effects of dielectric overlayers on structural and electronic properties. *ACS Nano* 4:2667–2672
122. Ahmed T, Biswas A, Subrina S (2021) Enhanced performance of strained graphene wrapped channel cylindrical FET. In: 2021 IEEE Region 10 Symposium (TENSYP), 1–4
123. Li P, Zeng RZ, Liao YB, Zhang QW, Zhou JH (2019) A novel graphene metal semi-insulator semiconductor transistor and its new super-low power mechanism. *Sci Rep* 9:3642
124. Withers F, Del Pozo-Zamudio O, Mishchenko A, Rooney AP, Gholinia A, Watanabe K, Taniguchi T, Haigh SJ, Geim AK, Tartakovskii AI, Novoselov KS (2015) Light-emitting diodes by band-structure engineering in van der Waals heterostructures. *Nat Mater* 14:301–306
125. Rodríguez-Mas F, Ferrer JC, Alonso JL, de Ávila SF, Valiente D (2021) Reduced graphene oxide inserted into PEDOT:PSS layer to enhance the electrical behaviour of light-emitting diodes. *Nanomaterials* 11:645
126. Yoo D, Lee K, Tchoe Y, Guha P, Ali A, Saroj RK, Lee S, Hamidul Islam ABM, Kim M, Yi G-C (2021) Dimension—and position-controlled growth of GaN microstructure arrays on graphene films for flexible device applications. *Sci Rep* 11, 17524
127. Chen Y-X, Lu D, Wang G-G, Huangfu J, Wu Q-B, Wang X-F, Liu L-F, Ye D-M, Yan B, Han J (2020) Highly efficient orange emissive graphene quantum dots prepared by acid-free method for white LEDs. *ACS Sustain Chem Eng* 8(17):6657–6666
128. Wang X, Tian H, Mohammad MA, Li C, Wu C, Yang Y, Ren T-L (2015) A spectrally tunable all-graphene-based flexible field-effect light-emitting device. *Nat Commun* 6:7767
129. Lim YS, Hung YM (2021) Anomalously enhanced light-emitting diode cooling via nucleate boiling using graphene-nanoplatelets coatings. *Energy Convers Manag* 244:114522
130. Bullock CJ, Bussy C (2019) Biocompatibility considerations in the design of graphene biomedical materials. *Adv Mater Interfaces* 6:1900229
131. Syama S, Mohanan PV (2016) Safety and biocompatibility of graphene: A new generation nanomaterial for biomedical application. *Int J Biol Macromol* 86:546–555
132. Torrente-Rodríguez RM, Lukas H, Tu J, Min J, Yang Y, Xu C, Rossiter HB, Gao W (2020) SARS-CoV-2 RapidPlex: A graphene-based multiplexed telemedicine platform for rapid and Low-Cost COVID-19 Diagnosis and Monitoring. *Matter* 3, 1981–1998
133. Molinero-Fernandez A, Arruza L, Lopez MA, Escarpa A (2020) On-the-fly rapid immunoassay for neonatal sepsis diagnosis: C-reactive protein accurate determination using magnetic graphene-based micromotors. *Biosens Bioelectron* 158:112156
134. Li G, Lu Z, Luan X, Wang Z, Liu F, Liu L (2021) Measurement method of akkermansia muciniphila by graphene-based transistor for diseases diagnosis. *IEEE Trans Nanotechnol* 20(1):332–337
135. Jeon J, Lee J, -in So J, Lee JB, Lee H, Chang Y, Shin S, Jo J, Ban C (2020) Homogeneous fluorescent aptasensor for active tuberculosis diagnosis by direct quantification of circulating TB7.7 based on aptamer beacon with graphene oxide. *Sens Actuators B Chem* 317, 128126
136. Siew QY, Pang EL, Loh H-S, Tan MTT (2021) Highly sensitive and specific graphene/TiO<sub>2</sub> impedimetric immunosensor based on plant-derived tetravalent envelope glycoprotein domain III (EDIII) probe antigen for dengue diagnosis. *Biosens Bioelectron* 176:112895
137. Afshar EG, Zarrabi A, Dehshahri A, Ashrafizadeh M, Dehghannoudeh G, Behnam B, Mandegary A, Pardakhty A, Mohammadinejad R, Tavakol S (2020) Graphene as a promising multifunctional nanoplatform for glioblastoma theranostic applications. *FlatChem* 22:100173
138. Majidi R, Nadafan M (2020) Detection of exhaled gas by  $\gamma$ -graphyne and twin-graphene for early diagnosis of lung cancer: A density functional theory study. *Phys Lett A* 384:126036
139. Nasrollahpour H, Isildak I, Rashidi M-R, Hashemi EA, Naseri A, Khalilzadeh B (2021) Ultrasensitive bioassaying of HER-2 protein for diagnosis of breast cancer using reduced graphene oxide/chitosan as nanobiocompatible platform. *Cancer Nano* 12:10
140. Barrera CC, Groot H, Vargas WL, Narváez DM (2020) Efficacy and molecular effects of a reduced graphene Oxide/Fe<sub>3</sub>O<sub>4</sub> nanocomposite in photothermal therapy against cancer. *Int J Nanomedicine* 15



141. Ardakania TS, Meidanchia A, Shokria A, Shakeri-Zadeh A (2020) Fe<sub>3</sub>O<sub>4</sub>@Au/reduced graphene oxide nanostructures: Combinatorial effects of radiotherapy and photothermal therapy on oral squamous carcinoma KB cell line. *Ceram Int* 46:28676–28685
142. Jia X, Xu W, Ye Z, Wang Y, Dong Q, Wang E, Li D, Wang J (2020) Functionalized graphene@gold nanostar/lipid for pancreatic cancer gene and photothermal synergistic therapy under photoacoustic/photothermal imaging dual-modal guidance. *Small* 16:2003707
143. Lima-Sousa R, de Melo-Diogo D, Alves CG, Cabral CSD, Miguel SP, Mendonça AG, Correia IJ (2020) Injectable in situ forming thermo-responsive graphene based hydrogels for cancer chemo-photothermal therapy and NIR light-enhanced antibacterial applications. *Mater Sci Eng C* 117:11129
144. Hao L, Song H, Zhan Z, Lv Y (2020) Multifunctional reduced graphene oxide-based nanoplatform for synergistic targeted chemo-photothermal therapy. *ACS Appl Bio Mater* 3:5213–5222
145. Yang S, Wang X, He P, Xu A, Wang G, Duan J, Shi Y, Ding G (2021) Graphene quantum dots with pyrrole N and pyridine N: Superior reactive oxygen species generation efficiency for metal-free sonodynamic tumor therapy. *Small* 17:2004867
146. Li Z, Wang D, Xu M, Wang J, Hu X, Anwar S, Tedesco AC, Moraisde PC, Bi H (2020) Fluorine-containing graphene quantum dots with a high singlet oxygen generation applied for photodynamic therapy. *J Mater Chem B* 8, 2598, 2606
147. Liu X, Yan B, Li Y, Ma X, Jiao W, Shi K, Zhang T, Chen S, He Y, Liang X-J, Fan H (2020) Graphene Oxide-Grafted Magnetic Nanorings Mediated Magnetothermodynamic Therapy Favoring Reactive Oxygen Species-Related Immune Response for Enhanced Antitumor Efficacy. *ACS Nano* 14:1936–1950
148. Raslan A, del Burgo LS, Ciriza J, Pedraz JL (2020) Graphene oxide and reduced graphene oxide-based scaffolds in regenerative medicine. *Int J Pharm* 580:119226
149. Bellet P, Gasparotto M, Pressi S, Fortunato A, Scapin G, Mba M, Menna E, Filippini F (2021) Graphene-Based scaffolds for regenerative medicine. *Nanomaterials* 11:404
150. Low FW, Lai CW, Abd Hamid SB (2017) Study of reduced graphene oxide film incorporated of TiO<sub>2</sub> species for efficient visible light driven dye-sensitized solar cell. *J Mater Sci: Mater Electron.* 28, 3819–3836
151. Sun S, Gao L, Liu Y (2010) Enhanced dye-sensitized solar cell using graphene- photoanode prepared by heterogeneous coagulation. *Appl Phys Lett* 96:083113
152. Basu K, Selopal GS, Mohammadnezad M, Akilimali R, Wang ZM, Zhao H, Vetrone F, Rosei F (2020) Hybrid graphene/metal oxide anodes for efficient and stable dye sensitized solar cell. *Electrochim Acta* 349:136409
153. Mustafa MN, Sulaiman Y (2020) Optimization of titanium dioxide decorated by graphene quantum dot as a light scatterer for enhanced dye-sensitized solar cell performance. *J Electroanal Chem* 876:114516
154. Casaluci S, Gemmi M, Pellegrini V, Carloa AD, Bonaccorso F (2016) Graphene-based large area dye-sensitized solar cell modules. *Nanoscale* 8:5368–5378
155. Oh WC, Cho KY, Jung CH, Areeerob Y (2020) Hybrid of Graphene based on quaternary Cu<sub>2</sub>ZnNiSe<sub>4</sub>-WO<sub>3</sub> Nanorods for Counter Electrode in Dye-sensitized Solar Cell Application. *Sci Rep* 10:4738
156. Miao X, Tongay S, Petterson MK, Berke K, Rinzler AG, Appleton BR, Hebard AF (2012) High efficiency graphene solar cells by chemical doping. *Nano Lett* 12:2745–2750
157. Wu J, Becerril HA, Bao Z, Liu Z, Chen Y, Peumans P (2008) Organic solar cells with solution-processed graphene transparent electrodes. *Appl Phys Lett* 92:263302
158. Ramli NF, Fahsyar PNA, Ludin NA, Teridi MAM, Ibrahim MA, Sepeai S (2021) Graphene dispersion as a passivation layer for the enhancement of perovskite solar cell stability. *Mater Chem Phys* 257:123798
159. Rehman MA, Roy SB, Gwak D, Akhtar I, Nasir N, Kumar S, Khan MF, Heo K, Chun S-H, Seo Y (2020) Solar cell based on vertical graphene nano hills directly grown on Silicon. *Carbon* 164:235–243

160. Lin T, Huang F, Lianga J, Wang Y (2011) A facile preparation route for boron-doped graphene, and its CdTe solar cell application. *Energy Environ Sci* 4:862–865
161. Wang C, Li D, Too CO, Wallace GG (2009) Electrochemical Properties of Graphene Paper Electrodes Used in Lithium Batteries. *Chem Mater* 21:2604–2606
162. Reddy ALM, Srivastava A, Gowda SR, Gullapalli H, Dubey M, Ajayan PM (2010) Synthesis of Nitrogen-Doped graphene films for lithium battery application. *ACS Nano* 4(11):6337–6342
163. Xiao J, Mei D, Li X, Xu W, Wang D, Graff GL, Bennett WD, Nie Z, Saraf LV, Aksay IA, Liu J, Zhang J-G (2011) Hierarchically porous graphene as a lithium-air battery electrode. *Nano Lett* 11:5071–5078
164. Shao G, Hanaor DAH, Wang J, Kober D, Li S, Wang X, Shen X, Bekheet MF, Gurlo A (2020) Polymer-Derived SiOC integrated with a graphene aerogel as a highly stable li-ion battery anode. *ACS Appl Mater Interfaces* 12:46045–46056
165. Han X, Zhang Z, Chen H, Zhang Q, Chen S, Yang Y (2020) On the interface design of si and multilayer graphene for a high-performance li-ion battery anode. *ACS Appl Mater Interfaces* 12:44840–44849
166. Ma T, Su TY, Zhang L, Yang J-W, Yao H-B, Lu L-L, Liu Y-F, He C, Yu S-H (2021) Scallion-Inspired graphene scaffold enabled high rate lithium metal battery. *Nano Lett* 21:2347–2355
167. Chen H, Guo F, Liu Y, Huang T, Zheng B, Ananth N, Xu Z, Gao W, Gao C (2017) A defect-free principle for advanced graphene cathode of aluminum-ion battery. *Adv Mater* 29:1605958
168. Chen H, Xu H, Wang S, Huang T, Xi J, Cai S, Guo F, Xu Z, Gao W, Gao C (2017) Ultrafast all-climate aluminum-graphene battery with quarter-million cycle life. *Sci Adv* 3, 12, eaao7233
169. Zhang J, Jiang J, Lib H, Zhao XS (2011) A high-performance asymmetric supercapacitor fabricated with graphene-based electrodes. *Energy Environ Sci* 4:4009–4015
170. Le LT, Ervin MH, Qiu H, Fuchs BE, Lee WY (2011) Graphene supercapacitor electrodes fabricated by inkjet printing and thermal reduction of graphene oxide. *Electrochem commun* 13:355–358
171. Fang Y, Luo B, Jia Y, Li X, Wang B, Song Q, Kang F, Zhi L (2012) Renewing Functionalized Graphene as Electrodes for High-Performance Supercapacitors. *Adv Mater* 24:6348–6355
172. Kim H, Park K-Y, Hong J, Kang K (2014) All-graphene-battery: bridging the gap between supercapacitors and lithium ion batteries. *Sci Rep* 4:5278
173. Guo H, Jiao T, Zhang Q, Guo W, Peng Q, Yan X. (2015) Preparation of graphene oxide-based hydrogels as efficient dye adsorbents for wastewater treatment. *Nanoscale Res Lett* 10, 272
174. Jiao T, Guo H, Zhang Q, Peng Q, Tang Y, Yan X, Li B (2015) Reduced graphene oxide-based silver nanoparticle-containing composite hydrogel as highly efficient dye catalysts for wastewater treatment. *Sci Rep* 5:11873
175. Zhong Y, Mahmud S, He Z, Yang Y, Zhang Z, Guo F, Chen Z, Xiong Z, Zhao Y (2020) Graphene oxide modified membrane for highly efficient wastewater treatment by dynamic combination of nanofiltration and catalysis. *J Hazard Mater* 397:122774
176. Ikram M, Raza A, Imran M, Ul-Hamid A, Shahbaz A, Ali S (2020) Hydrothermal synthesis of silver decorated reduced graphene oxide (rGO) nanoflakes with effective photocatalytic activity for wastewater treatment. *Nanoscale Res Lett* 15:95
177. Tabish TA, Memon FA, Gomez DE, Horsell DW, Zhang S (2018) A facile synthesis of porous graphene for efficient water and wastewater treatment. *Sci Rep* 8:1817
178. Zhao G, Li J, Ren X, Chen C, Wang X (2011) Few-Layered graphene oxide nanosheets as superior sorbents for heavy metal ion pollution management. *Environ Sci Technol* 45:10454–10462
179. Zhang K, Kemp KC, Chandra V (2012) Homogeneous anchoring of TiO<sub>2</sub> nanoparticles on graphene sheets for waste water treatment. *Mater Lett* 81:127–130
180. Marjani A, Nakhjiri AT, Adimi M, Jirandehi HF, Shirazian S (2020) Effect of graphene oxide on modifying polyethersulfone membrane performance and its application in wastewater treatment. *Sci Rep* 10:2049
181. Zhang J, Lu X, Shi C, Yan B, Gong L, Chen J, Xiang L, Xu H, Liu Q, Zeng H (2019) Unraveling the molecular interaction mechanism between graphene oxide and aromatic organic compounds with implications on wastewater treatment. *Chem Eng J* 358:842–849

182. Kumar V, Lee Y-S, Shin J-W, Kim K-H, Kukkar D, Tsang YF (2020) Potential applications of graphene-based nanomaterials as adsorbent for removal of volatile organic compounds. *Environ Int* 135:105356
183. Jung W, Jeong MH, Ahn KH, Kim T, Kim YH (2020) Reduced graphene-oxide filter system for removing filterable and condensable particulate matter from source. *J Hazard Mater* 391:122223
184. Tao L-Q, Zhang K-N, Tian H, Liu Y, Wang D-Y, Chen Y-Q, Yang Y, Ren T-L (2017) Graphene-paper pressure sensor for detecting human motions. *ACS Nano* 11:8790–8795
185. Pang Y, Zhang K, Yang Z, Jiang S, Ju Z, Li Y, Wang X, Wang D, Jian M, Zhang Y, Liang R, Tian H, Yang Y, Ren T-L (2018) Epidermis microstructure inspired graphene pressure sensor with random distributed spinosum for high sensitivity and large linearity. *ACS Nano* 12:2346–2354
186. Yang Z, Wang D-Y, Pang Y, Li Y-X, Wang Q, Zhang T-Y, Wang J-B, Liu X, Yang Y-Y, Jian J-M, Jian M-Q, Zhang Y-Y, Yang Y, Ren T-L (2018) Simultaneously detecting subtle and intensive human motions based on a silver nanoparticles bridged graphene strain sensor. *ACS Appl Mater Interfaces* 10:3948–3954
187. Yang Z, Pang Y, Han X-L, Yang Y, Ling J, Jian M, Zhang Y, Yang Y, Ren T-L (2018) Graphene textile strain sensor with negative resistance variation for human motion detection. *ACS Nano* 12:9134–9141
188. Qiao Y, Li X, Jian J, Wu Q, Wei Y, Shuai H, Hirtz T, Zhi Y, Deng G, Wang Y, Gou G, Xu J, Cui T, Tian H, Yang Y, Ren T-L (2020) Substrate-Free multilayer graphene electronic skin for intelligent diagnosis. *ACS Appl Mater Interfaces* 12:49945–49956
189. He J, Xiao P, Lu W, Shi J, Zhang L, Liang Y, Pan C, Kuo S-W, Chen T (2019) A Universal high accuracy wearable pulse monitoring system via high sensitivity and large linearity graphene pressure sensor. *Nano Energy* 59:422–433
190. Yang T, Jiang X, Zhong Y, Zhao X, Lin S, Li J, Li X, Xu J, Li Z, Zhu H (2017) A wearable and highly sensitive graphene strain sensor for precise home-based pulse wave monitoring. *ACS Sens.* 2:967–974
191. Liu W, Liu N, Yue Y, Rao J, Cheng F, Su J, Liu Z, Gao Y (2018) Piezoresistive pressure sensor based on synergistical innerconnect polyvinyl alcohol nanowires/wrinkled graphene film. *Small* 14:1704149
192. Prabhakaran A, Nayak P (2020) Surface engineering of laser-scribed graphene sensor enables nonenzymatic glucose detection in human body fluids. *ACS Appl Nano Mater* 3:391–398
193. Zhang Y, Li N, Xiang Y, Wang D, Zhang P, Wang Y, Lu S, Xu R, Zhao J (2020) A flexible non-enzymatic glucose sensor based on copper nanoparticles anchored on laser-induced graphene. *Carbon* 156:506–513
194. Zhenga Z, Wang H (2019) Different elements doped graphene sensor for CO<sub>2</sub> greenhouse gases detection: The DFT study. *Chem Phys Lett* 721:33–37
195. Seekaew Y, Wongchoosuk C (2019) A novel graphene-based electroluminescent gas sensor for carbon dioxide detection. *Appl Surf Sci* 479:525–531
196. Liu G, Tan Q, Kou H, Zhang L, Wang J, Lv W, Dong H, Xiong J (2018) A flexible temperature sensor based on reduced graphene oxide for robot skin used in internet of things. *Sensors* 18:1400
197. Davaji B, Cho HD, Malakoutian M, Lee J-K, Panin G, Kang TW, Lee CH (2017) A patterned single layer graphene resistance temperature sensor. *Sci Rep* 7, 8811
198. Yang J, Luo S, Zhou X, Li J, Fu J, Yang W, Wei D (2019) Flexible, tunable, and ultrasensitive capacitive pressure sensor with microconformal graphene electrodes. *ACS Appl Mater Interfaces* 11:14997–15006
199. Pang Y, Jian J, Tu T, Yang Z, Ling J, Li Y, Wang X, Qiao Y, Tian H, Yang Y, Ren T-L (2018) Wearable humidity sensor based on porous graphene network for respiration monitoring. *Biosens Bioelectron* 116:123–129
200. Liang C, Niu G, Chen X, Zhou Z, Yi Z, Ye X, Duan T, Yi Y, Xiao S (2019) Tunable triple-band graphene refractive index sensor with good angle-polarization tolerance. *Opt Commun* 436:57–62

201. Kaidarova A, Liu W, Swanepoel L, Almansouri A, Geraldi NR, Duarte CM, Kosel (2021) Flexible hall sensor made of laser-scribed graphene. *npj Flex. Electron.* 5, 2
202. Yu F, Camilli L, Wang T, Mackenzie DMA, Curioni M, Akid R, Bøggild P (2018) Complete long-term corrosion protection with chemical vapour deposited graphene. *Carbon* 132:78–84
203. Ghauri FA, Raza MA, Baig MS, Ibrahim S (2017) Corrosion study of the graphene oxide and reduced graphene oxide-based epoxy coatings. *Mater Res Express* 4:125601
204. Ye Y, Zhang D, Liu T, Liu Z, Pu J, Liu W, Zhao H, Li X, Wang L (2019) Superior corrosion resistance and self-healable epoxy coating pigmented with silanized trianiline-intercalated graphene. *Carbon* 142:164–176
205. Qiu S, Li W, Zheng W, Zhao H, Wang L (2017) Synergistic effect of polypyrrole-intercalated graphene for enhanced corrosion protection of aqueous coating in 3.5% NaCl Solution. *ACS Appl Mater Interfaces* 9, 34294–34304
206. Cui C, Lim ATO, Huang J (2017) A cautionary note on graphene anti-corrosion coatings. *Nat Nanotechnol* 12:834–835
207. Xu X, Yi D, Wang Z, Yu J, Zhang Z, Qiao R, Sun Z, Hu Z, Gao P, Peng H, Liu Z, Yu D, Wang E, Jiang Y, Ding F, Liu K (2018) Greatly enhanced anticorrosion of Cu by commensurate graphene coating. *Adv Mater* 30:1702944
208. Jin H, Zhang T, Bing W, Dong S, Tian L (2019) Antifouling performance and mechanism of elastic graphene–silicone rubber composite membranes. *J Mater Chem B* 7:488–497
209. Jin H, Bing W, Tian L, Wang P, Zhao J (2019) Combined effects of color and elastic modulus on antifouling performance: a study of graphene Oxide/Silicone Rubber Composite Membranes. *Materials* 12, 2608
210. Selim MS, Fathallah NA, Higazy SA, Hao Z, Mo PJ (2021) A comparative study between two novel silicone/graphene-based nanostructured surfaces for maritime antifouling. *J Colloid Interface Sci* 606:367–383
211. Jiang T, Qi L, Qin W (2019) Improving the environmental compatibility of marine sensors by surface functionalization with graphene oxide. *Anal Chem* 91:13268–13274
212. Fazli-Shokouhi S, Nasirpouri F, Khatamian M (2019) Polyaniline-modified graphene oxide nanocomposites in epoxy coatings for enhancing the anticorrosion and antifouling properties. *J Coat Technol Res* 16(4):983–997
213. Zhang W, Cheng W, Ziemann E, Be'er A, Lu X, Elimelech M, Bernstein R (2018) Functionalization of ultrafiltration membrane with polyampholyte hydrogel and graphene oxide to achieve dual antifouling and antibacterial properties. *J Membr Sci* 565, 293–302
214. Li X, Zhao W, Yin R, Huang X, Qian L (2018) A highly porous polyaniline-graphene composite used for electrochemical supercapacitors. *Eng Sci* 3, 89–95
215. Singh K, Ohlan A, Pham VH, Balasubramanian R, Varshney S, Jang J, Hur SH, Choi WM, Kumar M, Dhawan SK, Kong BS, Chung JS (2013) Nanostructured graphene/Fe<sub>3</sub>O<sub>4</sub> incorporated polyaniline as a high performance shield against electromagnetic pollution. *Nanoscale* 5, 2411
216. Kuila T, Bose S, Khanra P, Kim NH, Rhee KY, Lee JH (2011) Characterization and properties of in situ emulsion polymerized poly(methyl methacrylate)/graphene nanocomposites. *Compos Part A* 42:1856–1861
217. Thomassin J-M, Trifkovic M, Alkarmo W, Detrembleur C, Jerome C, Macosko C (2014) Poly(methyl methacrylate)/Graphene oxide nanocomposites by a precipitation polymerization process and their dielectric and rheological characterization. *Macromolecules* 47:2149–2155
218. Zabihi Z, Araghi H, Rodriguez PEDS, Boujakhrou A, Villalonga R (2019) Vapor sensing and interface properties of reduced graphene oxide–poly(methyl methacrylate) nanocomposite. *J Mater Sci: Mater Electron* 30, 2908–2919
219. Yuan X (2011) Enhanced interfacial interaction for effective reinforcement of poly(vinyl alcohol) nanocomposites at low loading of graphene. *Polym Bull* 67:1785–1797
220. Zhao X, Zhang Q, Chen D (2010) Enhanced mechanical properties of graphene-based poly(vinyl alcohol) composites. *Macromolecules* 43:2357–2363
221. Wang X, Liu X, Yuan H, Liu H, Liu C, Li T, Yan C, Yan X, Shen C, Guo Z (2018) Non-covalently functionalized graphene strengthened poly(vinyl alcohol). *Mater Des* 139:372–379

222. Zhou T, Chen F, Tang C, Bai H, Zhang Q, Deng H, Fu Q (2011) The preparation of high performance and conductive poly (vinyl alcohol)/graphene nanocomposite via reducing graphite oxide with sodium hydrosulfite. *Compos Sci Technol* 71:1266–1270
223. Li B, Luo J, Huang X, Lin L, Wang L, Hu M, Tang L, Xue H, Gao J, Mai Y-W (2020) A highly stretchable, super-hydrophobic strain sensor based on polydopamine and graphene reinforced nanofiber composite for human motion monitoring. *Compos Part B* 181:107580
224. Amani J, Maleki M, Khoshroo A, Sobhani-Nasab A, Rahimi-Nasrabadi M (2018) An electrochemical immunosensor based on poly p-phenylenediamine and graphene nanocomposite for detection of neuron-specific enolase via electrochemically amplified detection. *Anal Biochem* 548:53–59
225. Kumar SK, Castro M, Saiter A, Delbreilh L, Feller JF, Thomas S, Grohens Y (2013) Development of poly(isobutylene-co-isoprene)/reduced graphene oxide nanocomposites for barrier, dielectric and sensing applications. *Mater Lett* 96:109–112
226. Yu Z, Dai T, Yuan S, Zou H, Liu P (2020) Electromagnetic interference shielding performance of anisotropic polyimide/graphene composite aerogels. *ACS Appl Mater Interfaces* 12:30990–31001
227. Ganguly S, Ghosh S, Das P, Das TK, Ghosh SK, Das NC (2020) Poly(N-vinylpyrrolidone)-stabilized colloidal graphene-reinforced poly(ethylene-co-methyl acrylate) to mitigate electromagnetic radiation pollution. *Polym Bull* 77:2923–2943
228. Wang X, Yang H, Song L, Hu Y, Xing W, Lu H (2011) Morphology, mechanical and thermal properties of graphene-reinforced poly(butylene succinate) nanocomposites. *Compos Sci Technol* 72, 1–6
229. Hajian M, Reisi MR, Koohmareh GA, Jam ARZ (2012) Preparation and characterization of Polyvinylbutyral/Graphene Nanocomposite. *J Polym Res* 19:9966
230. Chen J, Ge J, Zhang L, Li Z, Li J, Sun Y, Qu L (2016) Reduced graphene oxide nanosheets functionalized with poly(styrene sulfonate) as a peroxidase mimetic in a colorimetric assay for ascorbic acid. *Microchim Acta* 183:1847–1853
231. Wu Y, Deng P, Tian Y, Feng J, Xiao J, Li J, Liu J, Li G, He Q (2020) Simultaneous and sensitive determination of ascorbic acid, dopamine and uric acid via an electrochemical sensor based on PVP-graphene composite. *J Nanobiotechnol* 18:112
232. Yasin G, Arif M, Nizam MN, Shakeel M, Khan MA, Khan WQ, Hassan TM, Abbas Z, Farahbakhsh I, Zuo Y (2018) Effect of surfactant concentration in electrolyte on the fabrication and properties of nickel-graphene nanocomposite coating synthesized by electrochemical co-deposition. *RSC Adv* 8:20039–20047
233. Jabbar A, Yasin G, Khan WQ, Anwar MY, Korai RM, Nizam MN, Muhyodin G (2017) Electrochemical deposition of nickel graphene composite coatings: effect of deposition temperature on its surface morphology and corrosion resistance. *RSC Adv* 7:31100–31109
234. Algul H, Tokur M, Ozcan S, Uysal M, Cetinkaya T, Akbulut H, Alp A (2015) The effect of graphene content and sliding speed on the wear mechanism of nickel-graphene nanocomposites. *Appl Surf Sci* 359:340–348
235. Xiang L, Shen Q, Zhang Y, Bai W, Nie C (2019) One-step electrodeposited Ni-graphene composite coating with excellent tribological properties. *Surf Coat Technol* 373:38–46
236. Hau TV, Trinh PV, Nam NPH, Tu NV, Lam VD, Phuong DD, Minh PN, Thang BH (2020) Electrodeposited nickel-graphene nanocomposite coating: effect of graphene nanoplatelet size on its microstructure and hardness. *RSC Adv* 10:22080–22090
237. Chang S-W, Nair AK, Buehler MJ (2013) Nanoindentation study of size effects in nickel-graphene nanocomposites. *Philos Mag Lett* 93(4):196–203
238. Chang S-W, Nair AK, Buehler MJ (2012) Geometry and temperature effects of the interfacial thermal conductance in copper—and nickel-graphene nanocomposites. *J Phys: Condens Matter* 24, 245301
239. Khobragade N, Sikdar K, Kumar B, Bera S, Roy D (2019) Mechanical and electrical properties of copper-graphene nanocomposite fabricated by high pressure torsion. *J Alloys Compd* 776:123–132

240. Wang S, Han S, Xin G, Lin J, Wei R, Lian J, Sun K, Zu X, Yu Q (2018) High-quality graphene directly grown on Cu nanoparticles for Cu-graphene nanocomposites. *Mater Des* 139:181–187
241. Pavithra CLP, Sarada BV, Rajulapati KV, Rao TN, Sundararajan G (2014) A new electrochemical approach for the synthesis of copper-graphene nanocomposite foils with high hardness. *Sci Rep* 4:4049
242. Huang J, Xie Z, Huang Y, Xie L, Luo S, Fan Q, Zeng T, Zhang Y, Wang S, Zhang M, Xie Z, Deng X (2020) Electrochemical immunosensor with Cu(I)/Cu(II)-chitosan-graphene nanocomposite-based signal amplification for the detection of newcastle disease virus. *Sci Rep* 10:13869
243. Shabnam L, Faisal SN, Roy AK, Haque E, Minett AI, Gomes VG (2017) Doped graphene/Cu nanocomposite: A high sensitivity non-enzymatic glucose sensor for food. *Food Chem* 221:751–759
244. Yuan W, Gu Y, Li L (2012) Green synthesis of graphene/Ag nanocomposites. *Appl Surf Sci* 261:753–758
245. Khan ME, Khan MM, Cho MH (2015) Biogenic synthesis of a Ag–graphene nanocomposite with efficient photocatalytic degradation, electrical conductivity and photoelectrochemical performance. *New J Chem* 39:8121–8129
246. Shen J, Shi M, Li N, Yan B, Ma H, Hu Y, Ye M (2010) Facile synthesis and application of ag-chemically converted graphene nanocomposite. *Nano Res* 3:339–349
247. Pasricha R, Gupta S, Srivastava AK (2009) A facile and novel synthesis of ag–graphene-based nanocomposites. *Small* 5(20):2253–2259
248. Wang P, Liu Z-G, Chen X, Meng F-L, Liu J-H, Huang X-J (2013) UV irradiation synthesis of an Au–graphene nanocomposite with enhanced electrochemical sensing properties. *J. Mater. Chem. A* 1:9189
249. Khan ME, Khan MM, Cho MH (2015) Green synthesis, photocatalytic and photoelectrochemical performance of an Au–Graphene nanocomposite. *RSC Adv* 5:26897–26904
250. Govindhan M, Amiri M, Chen A (2015) Au nanoparticle/graphene nanocomposite as a platform for the sensitive detection of NADH in human urine. *Biosens Bioelectron* 66:474–480
251. Çiplak Z, Yıldız N, Çalimli Ay (2015) Investigation of graphene/ag nanocomposites synthesis parameters for two different synthesis methods. *Fuller Nanotub Carbon Nanostructures* 23, 4, 361–370
252. Tahernejad-Javazmi F, Shabani-Nooshabadi M, Karimi-Maleh H (2019) 3D reduced graphene oxide/FeNi<sub>3</sub>-ionic liquid nanocomposite modified sensor; an electrical synergic effect for development of tert-butylhydroquinone and folic acid sensor. *Compos Part B* 172:666–670
253. Vengatesan MR, Darawsheh IFF, Govindan B, Alhseinat E, Banat F (2019) Ag-Cu bimetallic nanoparticle decorated graphene nanocomposite as an effective anode material for hybrid capacitive deionization (HCDI) System. *Electrochim Acta* 297:1052–1062
254. Zhang Y, Tang Z-R, Fu X, Xu Y-J (2010) TiO<sub>2</sub>-Graphene nanocomposites for gas-phase photocatalytic degradation of volatile aromatic pollutant: Is TiO<sub>2</sub>-Graphene truly different from other TiO<sub>2</sub>-Carbon composite materials? *ACS Nano* 4(12):7303–7314
255. Zhang Y, Tang Z-R, Fu X, Xu Y-J (2011) Engineering the unique 2D mat of graphene to achieve graphene-TiO<sub>2</sub> nanocomposite for photocatalytic selective transformation: what advantage does graphene have over its forebear carbon nanotube? *ACS Nano* 5(9):7426–7435
256. Qiu J, Lai C, Wang Y, Li S, Zhang S (2014) Resilient mesoporous TiO<sub>2</sub>/graphene nanocomposite for high rate performance lithium-ion batteries. *Chem Eng J* 256:247–254
257. Le Z, Liu F, Nie P, Li X, Liu X, Bian Z, Chen G, Wu HB, Lu Y (2017) Pseudocapacitive sodium storage in mesoporous single-crystal-like TiO<sub>2</sub>–Graphene nanocomposite enables high performance sodium-ion capacitors. *ACS Nano* 11:2952–2960
258. Fan Y, Lu H-T, Liu J-H, Yang C-P, Jing Q-S, Zhang Y-X, Yang X-K, Huang K-J (2011) Hydrothermal preparation and electrochemical sensing properties of TiO<sub>2</sub>–graphene nanocomposite. *Colloids Surf B: Biointerfaces* 83:78–82
259. Lee S, Oh J, Kim D, Piao Y (2016) A sensitive electrochemical sensor using an iron oxide/graphene composite for the simultaneous detection of heavy metal ions. *Talanta* 160:528–536

260. Sua H, Ye Z, Hmidi N (2017) High-performance iron oxide–graphene oxide nanocomposite adsorbents for arsenic removal. *Colloids and Surfaces A: Physicochem. Eng. Aspects* 522, 161–172
261. Yuan Y, Jiang W, Wang Y, Shen P, Li F, Li P, Zhao F, Gao H (2014) Hydrothermal preparation of Fe<sub>2</sub>O<sub>3</sub>/graphene nanocomposite and its enhanced catalytic activity on the thermal decomposition of ammonium perchlorate. *Appl Surf Sci* 303:354–359
262. Xiao L, Schroeder M, Kluge S, Balducci A, Hagemann U, Schulz C, Wiggers H (2015) Direct self-assembly of Fe<sub>2</sub>O<sub>3</sub>/reduced graphene oxide nanocomposite for high-performance lithium-ion batteries. *J Mater Chem A* 3:11566–11574
263. Jiang W, Liang F, Wang J, Su L, Wu Y, Wang L (2014) Enhanced electrochemical performances of FeOx–graphene nanocomposites as anode materials for alkaline nickel–iron batteries. *RSC Adv* 4:15394–15399
264. Ren H, Bai Y, Wang X, Ni Q, Wang Z, Li Y, Chen G, Wu F, Xu H, Wu C (2019) High-Capacity interstitial Mn-Incorporated MnFe<sub>3–x</sub>O<sub>4</sub>/Graphene nanocomposite for sodium-ion battery anodes. *ACS Appl Mater Interfaces* 11:37812–37821
265. Liang C, Song P, Ma A, Shi X, Gub H, Wang L, Qiu H, Kong J, Gu J (2019) Highly oriented three-dimensional structures of Fe<sub>3</sub>O<sub>4</sub> decorated CNTs/reduced graphene oxide foam/epoxy nanocomposites against electromagnetic pollution. *Compos Sci Technol* 181:107683
266. Shen B, Zhai W, Tao M, Ling J, Zheng W (2013) Lightweight, multifunctional polyetherimide/graphene@Fe<sub>3</sub>O<sub>4</sub> composite foams for shielding of electromagnetic pollution. *ACS Appl Mater Interfaces* 5:11383–11391
267. Wang B, Wu X-L, Shu C-Y, Guo Y-G, Wang C-R (2010) Synthesis of CuO/graphene nanocomposite as a high-performance anode material for lithium-ion batteries. *J Mater Chem* 20:10661–10664
268. Rai AK, Anh LT, Gim J, Mathew V, Kang J, Paul BJ, Singh NK, Song J, Kim J (2013) Facile approach to synthesize CuO/reduced graphene oxide nanocomposite as anode materials for lithium-ion battery. *J Power Sources* 244:435–441
269. Perreault LL, Colò F, Meligrana G, Kim K, Fiorilli S, Bella F, Nair JR, Vitale-Brovarone C, Florez J, Kleitz F, Gerbaldi C (2018) Spray-Dried mesoporous mixed Cu-Ni Oxide@Graphene nanocomposite microspheres for high power and durable li-ion battery anodes. *Adv Energy Mater* 8:1802438
270. Orhan Z, Cınan E, Çaldıran Z, Kurucu Y, Daş E (2020) Synthesis of CuO–graphene nanocomposite material and the effect of gamma radiation on CuO–graphene/p-Si junction diode. *J Mater Sci: Mater Electron* 31, 12715–12724
271. Luo L, Zhu Li, Wang Z (2012) Nonenzymatic amperometric determination of glucose by CuO nanocubes–graphene nanocomposite modified electrode. *Bioelectrochemistry* 88, 156–163
272. Gayathri S, Jayabal P, Kottaisamy M, Ramakrishnan V (2014) Synthesis of ZnO decorated graphene nanocomposite for enhanced photocatalytic properties. *J Appl Phys* 115:173504
273. Lonkar SP, Pillai V, Abdala A (2019) Solvent-free synthesis of ZnO-graphene nanocomposite with superior photocatalytic activity. *Appl Surf Sci* 465:1107–1113
274. Yukird J, Kongsittikul P, Qin J, Chailapakul O, Rodthongkum N (2018) ZnO@graphene nanocomposite modified electrode for sensitive and simultaneous detection of Cd (II) and Pb (II). *Synth Met* 245:251–259
275. Anand K, Singh O, Singh MP, Kaur J, Singh RC (2014) Hydrogen sensor based on graphene/ZnO nanocomposite. *Sens. Actuator B* 195:409–415
276. Jayabal P, Gayathri S, Sasirekha V, Mayandi J, Ramakrishnan V (2014) Preparation and characterization of ZnO/graphene nanocomposite for improved photovoltaic performance. *J Nanopart Res* 16:2640
277. Moradi S, Sobhgol SA, Hayati F, Isari AA, Kakavandi B, Bashardoust P, Anvaripour B (2020) Performance and reaction mechanism of MgO/ZnO/Graphene ternary nanocomposite in coupling with LED and ultrasound waves for the degradation of sulfamethoxazole and pharmaceutical wastewater. *Sep Purif Technol* 251:117373
278. Chen W, Song K, Mi L, Feng X, Zhang J, Cui S, Liu C (2017) Synergistic effect induced ultrafine SnO<sub>2</sub>/graphene nanocomposite as an advanced lithium/sodium-ion batteries anode. *J. Mater. Chem. A* 5, 10027-10038

279. Su D, Ahn H-J, Wang G (2013) SnO<sub>2</sub>@graphene nanocomposites as anode materials for Na-ion batteries with superior electrochemical performance. *Chem Commun* 49:3131–3133
280. Zhang D, Chang H, Li P, Liu R, Xue Q (2016) Fabrication and characterization of an ultrasensitive humidity sensor based on metal oxide/graphene hybrid nanocomposite. *Sens Actuators B* 225:233–240
281. Zhang M, Lei D, Yu X, Chen L, Li Q, Wang Y, Wang T, Cao G (2012) Graphene oxide oxidizes stannous ions to synthesize tin sulfide–graphene nanocomposites with small crystal size for high performance lithium ion batteries. *J Mater Chem* 22:23091–23097
282. Ma T, Sun L, Niu Q, Xu Y, Zhu K, Liu X, Guo X, Zhang J (2019) N-doped carbon-coated Tin sulfide/graphene nanocomposite for enhanced lithium storage. *Electrochim Acta* 300:131–137
283. Shi J, Wang Y, Su Q, Cheng F, Kong X, Lin J, Zhu T, Liang S, Pan A (2018) N-S co-doped C@SnS nanoflakes/graphene composite as advanced anode for sodium-ion batteries. *Chem Eng J* 353:606–614
284. Yang B, Zuo X, Chen P, Zhou L, Yang X, Zhang H, Li G, Wu M, Ma Y, Jin S, Chen X (2015) Nanocomposite of tin sulfide nanoparticles with reduced graphene oxide in high-efficiency dye-sensitized solar cells. *ACS Appl Mater Interfaces* 7:137–143
285. Wu J, Wu Z, Ding H, Wei Y, Huang W, Yang X, Li Z, Qiu L, Wang X (2020) Flexible, 3D SnS<sub>2</sub>/Reduced graphene oxide heterostructured NO<sub>2</sub> sensor. *Sens Actuators B: Chem* 305:127445
286. Johnny J, Sepulveda-Guzman S, Krishnan B, Avellaneda DA, Aguilar Martinez JA, Anantharaman MR, Shaji S (2019) Tin sulfide: Reduced graphene oxide nanocomposites for photovoltaic and electrochemical applications. *Sol Energy Mater Sol Cells* 189, 53–62
287. Kapadnis RS, Bansode SB, Supekar AT, Bhujbal PK, Kale SS, Jadar SR, Pathan HM (2020) Cadmium telluride/cadmium sulfide thin films solar cells: a review. *ES Energy Environ* 10:3–12
288. Zeng P, Zhang Q, Peng T, Zhang X (2011) One-pot synthesis of reduced graphene oxide–cadmium sulfide nanocomposite and its photocatalytic hydrogen production. *Phys Chem Chem Phys* 13:21496–21502
289. Peng T, Li K, Zeng P, Zhang Q, Zhang X (2012) Enhanced photocatalytic hydrogen production over graphene oxide–cadmium sulfide nanocomposite under visible light irradiation. *J Phys Chem C* 116:22720–22726
290. Alhammadi S, Minnam Reddy VR, Gedi S, Park H, Sayed MS, Shim J-J, Kim WK (2020) Performance of Graphene–CdS hybrid nanocomposite thin film for applications in Cu(In,Ga)Se<sub>2</sub> Solar Cell and H<sub>2</sub> Production. *Nanomaterials* 10, 245
291. Ge L, Hong Q, Li H, Liu C, Li F (2019) Direct-Laser-Writing of metal sulfide-graphene nanocomposite photoelectrode toward sensitive photoelectrochemical sensing. *Adv Funct Mater* 29:1904000
292. Roshan H, Sheikhi MH, Faramarzi Haghighi MK, Padidar P (2020) High-Performance room temperature methane gas sensor based on lead sulfide/reduced graphene oxide nanocomposite. *IEEE Sens. J.* 20, 5
293. Qu B, Chen Y, Zhang M, Hu L, Lei D, Lu B, Li Q, Wang Y, Chen L, Wang T (2012) β-Cobalt sulfide nanoparticles decorated graphene composite electrodes for high capacity and power supercapacitors. *Nanoscale* 4:7810–7816
294. Zhu J, Zhou W, Zhou Y, Cheng X, Yang J (2019) Cobalt sulfide/reduced graphene oxide nanocomposite with enhanced performance for supercapacitors. *J Electron Mater* 48:1531–1539
295. Ramachandran R, Felix S, Saranya M, Santhosh C, Velmurugan V, Chakkravarthy Ragupathy BP, Jeong SK, Grace AN (2013) Synthesis of cobalt sulfide-graphene (CoS/G) nanocomposites for supercapacitor applications. *IEEE Trans. Nanotechnol.* 12, 6, 985–990
296. Huang G, Chen T, Wang Z, Chang K, Chen W (2013) Synthesis and electrochemical performances of cobalt sulfides/graphene nanocomposite as anode material of Li-ion battery. *J Power Sources* 235:122–128
297. Prasad J, Singh AK, Yadav AN, Kumar A, Tomar M, Srivastava A, Kumar P, Gupta V, Singh K (2020) Molybdenum disulfide-wrapped carbon nanotube-reduced graphene oxide



- (CNT/MoS<sub>2</sub>-rGO) nanohybrids for excellent and fast removal of electromagnetic interference pollution. *ACS Appl Mater Interfaces* 12:40828–40837
298. Khan M, Yousaf AB, Chen M, Wei C, Wu X, Huang N, Qi Z, Li L (2016) Molybdenum sulfide/graphene-carbon nanotube nanocomposite material for electrocatalytic applications in hydrogen evolution reactions. *Nano Res* 9(3):837–848
  299. Peng W, Wang W, Han G, Huang Y, Zhang Y (2020) Fabrication of 3D flower-like MoS<sub>2</sub>/graphene composite as high-performance electrode for capacitive deionization. *Desalination* 473:114191
  300. Yang YJ, Li W, Wu X (2014) Copper sulfide/reduced graphene oxide nanocomposite for detection of hydrazine and hydrogen peroxide at low potential in neutral medium. *Electrochim Acta* 123:260–267
  301. Shi F, Zheng W, Wang W, Hou F, Lei B, Sun Z, Sun W (2015) Application of graphene-copper sulfide nanocomposite modified electrode for electrochemistry and electrocatalysis of haemoglobin. *Biosens Bioelectron* 64:131–137
  302. Wang A, Wang H, Zhang S, Mao C, Song J, Niu H, Jin B, Tian Y (2013) Controlled synthesis of nickel sulfide/graphene oxide nanocomposite for high-performance supercapacitor. *Appl Surf Sci* 282:704–708
  303. Xing Z, Chu Q, Ren X, Tian J, Asiri AM, Alamry KA, Al-Youbi AO, Sun X (2013) Biomolecule-assisted synthesis of nickel sulfides/reduced graphene oxide nanocomposites as electrode materials for supercapacitors. *Electrochem Commun* 32:9–13
  304. Huang K-J, Wang L, Liu Y-J, Gan T, Liu Y-M, Wang L-L, Fan Y (2013) Synthesis and electrochemical performances of layered tungsten sulfide-graphene nanocomposite as a sensing platform for catechol, resorcinol and hydroquinone. *Electrochim Acta* 107:379–387
  305. Wu D, Wang C, Wu M, Chao Y, He P, Ma J (2020) Porous bowl-shaped VS<sub>2</sub> nanosheets/graphene composite for high-rate lithium-ion storage. *J Energy Chem* 43:24–32